C.P. No. 1239

C.P. No. 1239

MINISTRY OF DEFENCE (PROCUREMENT EXECUTIVE)

AERONAUTICAL RESEARCH COUNCIL

CURRENT PAPERS

Measurements of Temperature and Pressure behind the Incident and Reflected Shocks in a Shock Tube

By

Michael J. Lewis and Leonard Bernstein

Queen Mary College, University of London

LONDON: HER MAJESTY'S STATIONERY OFFICE

1973

Price 80p net

CP No. 1239*
March, 1972

MEASUREMENTS OF TEMPERATURE AND PRESSURE BEHIND THE INCIDENT AND REFLECTED SHOCKS IN A SHOCK TUBE

- By -

Michael J. Lewis and Leonard Bernstein
Queen Mary College, University of London

SUMMARY

The many perturbing mechanisms in a shock tube flow and the problems involved in predicting their effects make it essential to calibrate a shock tube over its working range. Pressure and temperature measurements behind the incident shock and in the reflected shock region are presented for the QMC 38.1 mm square-channel shock-tube using hydrogen driving shocks into nitrogen. Some temperature measurements were also made at the entrance to a convergent-divergent nozzle. The incident shock Mach number range is between 3.5 and 7. These measurements indicate that temperature gradients are present in the shocked gas and that the high temperature duration of the shocked gas is less than the steady pressure duration and is very much smaller than that predicted using ideal gas wave theory.

*Replaces A.R.C.33 776

Contents

1. Introduction

The ideal wave system, which is illustrated in figure 1, and the gas flow conditions generated in a simple shock-tube are well-known and well-documented (Glass & Hall, 1959). In reality, departures from this ideal behaviour occur. Boundary layer growth (Mirels, 1971), non-instantaneous diaphragm opening (Simpson et al, 1967), contact-surface mixing (Hooker, 1961) and non-equilibrium effects (Spence, 1961) cause the velocity of the incident shock wave to vary. Thermal gradients appear in the shocked gas and large reductions in 'testing time' occur. In the region behind the reflected shock front these departures from the ideal are enhanced by the complicated interactions which take place between the reflected-shock and both the contact-region (Rudinger, 1961) and boundary-layer (Davies, 1965 & Allen, 1968). Although these real gas effects, which should not be confused with thermal or caloric imperfections, are also well-known, they are by no means completely predictable. Hence to establish with any certainty the way in which conditions in a shock-tube vary with time, it is necessary to calibrate the device over its working range. In this way suitable measurements determine the overall effect of the perturbing mechanisms (or 'real gas effects') and complex, uncertain analyses are avoided.

The purpose of this report is to present a calibration for the 38.1 mm square-channel shock-tube at Queen Mary College. A series of pressure and temperature measurements behind the incident shock front and in the reflected shock region was carried out. It is hoped that these measurements provide sufficient information for this particular shock tube to be used to carry out aerodynamic or chemical experiments. No attempt has been made to compare the experimental results quantitatively with the many theoretical models which have been proposed to account for the deviations from the ideal. The results are compared only with the predictions of ideal theory.

2. The shock-tube and measuring equipment

The Queen Mary College 38.1 mm square-channel shock-tube is described by Ackroyd (1964). Its test-section, which is attached to the end of the channel, is shown in figure 2. Windows or transducers may be mounted in the ports available in this section. An end-plate may be placed in the shock-tube channel for investigating the reflected shock region. The plate and supporting assembly are shown in figure 3. As an alternative to this plate, two steel inserts may be mounted to form a two-dimensional nozzle, whose dimensions are given in figure 4. Multimorph* piezoelectric elements are flush-mounted at various stations along the shock-tube channel. They are used as shock detectors and their mountings and associated trigger amplifiers are described by Bernstein & Goodchild (1967).

The pressure variations behind the incident shock wave and in the reflected shock region were measured with a Kistler type 701A pressure transducer and an MQ 20 pressure transducer respectively. A double-beam single-source sodium line-reversal system was used to measure the vibrational temperature T_v, of the shocked gas. This technique is described by Gaydon and Hurle (1963) and the sodium introductory system is described by Lewis et al (1969). The optical system is depicted schematically in figure 5. It is estimated that with this line-reversal system the vibrational temperature of the test gas may be measured to within $\pm$ 25 K, provided that the brightness temperature of the background source is greater than the vibrational temperature of the test gas. Both the temperature and pressure signals were displayed on oscilloscopes and recorded on Polaroid film.

The shock tube was operated with hydrogen driving shocks into nitrogen, both initially at room temperature. The diaphragm material in most of the experiments was 'Melinex'. Several experiments were carried out with scored aluminium diaphragms.

3. Temperature and pressure measurements behind the incident shock wave

Temperature and pressure measurements behind the incident shocks in nitrogen were made at station m. The shock-tube stations are indicated in figure 2. Shock transit times between stations 1 and n, and between

---

* Brush Clevite trade name

i and j, were measured to determine the local shock Mach number $W(X_m)$, at station m. These measurements also supplied information on the shock attenuation present in this tube. This attenuation was in close agreement with that measured by Bernstein (1963 a).

Four typical vibrational temperature variations as a function of trace time t, are shown in figure 6, together with a typical oscillogram. The initial channel pressure p_1, and the brightness temperature T_L of the lamp used in the line-reversal system are indicated for each test. The size of the data points is an indication of the estimated uncertainty in the temperature. On the oscillogram, points S and C respectively indicate the shock and contact-region arrival at the measuring station. Arrows 'e' and 'a' respectively indicate the emission signal from the sodium atoms and the absorption of these atoms relative to the background source.

It is not clear from these curves how far the vibrational energy non-equilibrium region of the shocked flow extends behind the shock front. Temperature gradients, caused by real gas effects in the shocked flow, cannot be separated directly from vibrational temperature gradients caused by the relaxation process. To clarify the situation, the particle time t_p and the local temperature T of the active mode were calculated at each datum point. Corrections for shock attenuation were applied as described in Appendix A. The results of these calculations are shown in figure 7. The relaxation zone and the thermal gradients are clearly seen. The equilibrium temperature T_2 is based upon the shock strength $W(X_m)$ at station m. A temperature difference of approximately 200 K exists between this temperature and that measured at the front of the contact region. Similar differences were found to exist over the whole range of measurements. This is shown in figure 8, where the measured temperatures near the contact region (i.e. at point C on each oscillogram) are plotted as a function of $W(X_m)$ and compared with T_2. It is also evident from the scatter in this figure that the repeatability of the shock tube flow is poor. The scatter, which is assumed to be caused by the difficulty of controlling the diaphragm bursting, was reduced by placing an arbitrary limit on the results; two lines, which embraced the majority of the measured points, were drawn. Tests which fell outside these lines were discarded.

The influence of the real gas effects upon the hot flow duration or testing time, that is, the time between points S and C on the oscillograms, is shown in figure 9, where this time is plotted as a function of $W(X_m)$. Included are similar times calculated using boundary layer theory (Mirels, 1971) and using ideal theory. The former gives a very reasonable estimate of the testing time, whilst the latter overestimates this time by a factor of five. A time, determined from a schlieren picture of the shocked gas, is shown at $W(X_m) = 5.5$.

The measured thermal gradients evident in the shocked gas region suggest that similar gradients in pressure would be present behind the incident shock. Four typical pressure oscillograms are shown in figure 10. The traces are characterised by a sharp initial rise in pressure across the shock wave, a region of fairly steady or slowly falling pressure, up to a point labelled H, and by an increase in pressure after point H. Transducer ringing on the pressure signals was reduced considerably by using an electronic filter, but at the expense of response. The pressures were measured from each oscillogram at points S and H. The results from all tests, non-dimensionalised in terms of p_1, are shown in figure 11 where the pressure ratios P_{S1} and P_{H1} are plotted as a function of $W(X_m)$. The theoretical shock pressure ratio P_{21} calculated from imperfect gas theory (Bernstein 1963 b) is also indicated. The agreement between the measured and theoretical shock pressure ratios and the scatter around the theoretical curve at the upper end of the shock Mach number range suggest that the slight fall in pressure noted in the measurements may not in fact occur. It is possibly the combined effect of the electronic filtering and some thermal response of the pressure gauge.

The pressure rise after point H is not explained so lightly. Such increases in pressure have been noted by Wittliff and Wilson (1957). The duration of the fairly steady pressure region up to point H is shown in figure 12 as a function of $W(X_m)$, together with the hot flow duration taken from figure 9. Curve F represents the arrival at the measuring station of the tail R_T of the rarefaction wave shed at diaphragm burst. R_T is shown in figure 1. Curve F was calculated using the ideal data given by Glass & Hall (1959) slightly modified to account for shock attenuation. Figure 12 shows that the increase in pressure subsequent to H occurs after the front of the contact region arrives at the measuring station. It is

not then associated with the measured temperature gradients. A combination of boundary layer effects, the expansion wave shed from the diaphragm and diaphragm opening phenomena probably causes this pressure to rise. However, this rise in pressure does not affect the hot flow behind the incident shock wave. It may have some effect on the latter part of the hot flow duration in the reflected shock region.

As a by-product of the vibrational temperature measurements, normalised vibrational energy relaxation times or napier times (τ_N) were determined by locally integrating the Bethe-Teller rate equation (Johanneson, 1961). The results are presented in figure 13, where τ_N is shown as a function of the local temperature T of the active modes. The vertical bars indicate the variation in relaxation time obtained from each experiment and the circles are a mean of the relaxation data. The times are in reasonable agreement with those obtained by other workers (see for example, Sebacher, 1967), showing a tendency towards the low temperature correlation of Huber & Kantrowitz (1947), rather than that of Russo & Watt (1968).

4. Temperature and pressure measurements in the reflected shock region

4.1 Measurements near a reflecting plate

The reflecting plate was mounted in the test section, as shown in figure 3, 25.4 mm from station m. Pressure measurements were made at the plate using the MQ 20 gauge and temperature measurements were made simultaneously at station m, using the sodium line reversal system, over the range $3.0 < W(X_m) < 7.5$. Above an incident shock Mach number of about 4.8, the gas temperature exceeded the maximum brightness temperature (2910 K) of the lamp. Under these circumstances uncertainties in the measured temperatures became large. The experiments are therefore divided into three groups as follows.

1. Experiments with $W(X_m) < 5$ and the lamp brightness temperature not exceeding 2910 K.
2. Experiments with $W(X_m) > 5$ and a lamp brightness temperature of 2910 K. These measurements gave an indication of the hot flow duration in the reflected shock region.
3. Since experiments in groups 1 and 2 only covered the relatively short high temperature duration in the reflected shock region, several experiments were carried out with a relatively slow oscilloscope sweep rate. These are called 'long time' measurements.

Typical temperature and pressure (p) variations as a function of time are shown in figures 14 and 15 together with a typical temperature oscillogram. Arrow S_R marks the arrival of the reflected shock at station m and S marks the arrival of the incident shock at the reflecting plate. It is seen that the shape of the temperature and corresponding pressure curves are similar but they are displaced in time because the temperature and pressure measuring stations are 25.4 mm.apart. The same waves arrive at each station, but at different times.

The pressure variations show an initial jump in pressure to point A, followed by a slow increase in pressure to a stationary value at B. The pressure then falls to a 'minimum' at C and rises to a maximum again at D. The pressure at A, normalised in terms of the initial channel pressure, is designated P_{A1}. Similar pressures P_{B1}, P_{C1} and P_{D1} are defined. The time measured from S to point B is t_B, and similar times are defined for C and D. There is an initial rise in temperature, associated with the vibrational energy relaxation region, to a steady value. Because of the relaxation zone, no points on the temperature curves are defined corresponding to A and B on the pressure curves. The temperature rises from point c, after the steady value, to a maximum at d, after which a temperature fall occurs. A point g is defined at which the temperature has again reached its value at c. The temperature at c is T_c and similar temperatures T_d and T_g are defined. The time measured from S_R on the oscillograms to c is t_c, and similar times are defined for points d and g.

Typical 'long time' temperature and pressure oscillograms are shown in figure 16. On the temperature oscillogram two points 1 and f are shown. Point 1 corresponds to a reversal condition at which the gas temperature equals the lamp brightness temperature (2910 K). Point f and the time t_f indicate when the emission from the gas has fallen to zero. This indicates a relatively low temperature in the reflected shock region. A point E is chosen on the pressure oscillogram at which the pressure starts to fall at the reflecting plate after a comparatively long period of reasonably steady pressure.

An attempt was made to correlate the reflected shock measurements, which are summarised in figures 17 to 21, with ideal predictions based upon $W(X_m)$. The reflected-shock pressure ratio P_{51} and the temperature T_5 behind the reflected shock were taken from the tables of Bernstein (1963 b). There is good correspondence between P_{51} and P_{A1}, but poor agreement is found between T_5 and T_c. This is to be expected since

some allowance needs to be made for the displacement of station m from the reflecting plate and the longitudinal temperature gradient in the reflected shock region; the temperature gradient evident behind the incident shock is magnified in the reflected shock region. The equilibrium temperature at station m was re-estimated (see Appendix B for details) using the incident shock results described in Section 3. This corrected temperature is seen to be in reasonable agreement with T_c. At times later than t_C (or t_c) the measured variations in pressure and temperature do not correspond with those predicted by the ideal model of shock tube behaviour. The major deficiency of this model is its failure to account for the behaviour of the contact surface or interface between the driver and driven gases. It is well known that this interface spreads fairly rapidly to form a region several shock tube diameters in length and this travels along the channel of the shock tube rather more quickly than ideal theory would indicate. This accounts for the curtailment of the hot flow duration in the region behind the primary front. When this shock reflects from the end wall of the shock tube it consequently meets the contact region much sooner than is predicted by ideal theory. Moreover the initial stages of the interaction between the reflected shock and the contact region will be similar to that which takes place with a 'weak' contact discontinuity, that is, one with a small internal energy difference across it.

It is not difficult to show (see Teague, 1968) that for the special case in which the specific heat capacity ratio γ remains constant through the contact region, the strength δp of the wave reflected from the interaction of a shock with an infinitesimal element of contact region is given by

$$\frac{a_2}{p_s}\frac{\delta p}{\delta a} = -\left\{\frac{\left[\beta(1+\alpha P_{25})\right]^{\frac{1}{2}}}{1-P_{25}} + \frac{1}{1-P_{25}} - \frac{\alpha}{2(\alpha+P_{25})}\right\}^{-1}$$

where δa is the change in acoustic speed through the element and α and β are functions of γ (see Notation).
The right hand side of this equation is always negative*, so the sign of δp depends only upon that of δa. Since the acoustic velocity in the contact region depends upon the ratio of the temperature to the average local molecular mass, both of which vary in the present experiments, the

---

* The range $(\alpha+2)^{-1} \leq P_{25} \leq 1$ covers all possible reflected shocks in a shock tube, assuming perfect gases.

initial reflected wave is of undetermined sign. When $\delta\alpha$ is negative initially (that is, at the 'hot end' of the contact region in a shock tube) a compression is first reflected, and vice versa. However, Chisnell (1955) has shown that the overall strength of the wave reflected from an interaction with a contact region is the same as that reflected from an ideal contact surface with the same internal energy ratio across it. Viewed in this light the pressure traces such as those indicated in figures 14 to 18 may be interpreted in the following manner. At time t_B the first wave reflected from the interaction between the reflected shock and the front of the contact region arrives at the end plate. One would infer that at the front of the contact region $\delta\alpha$ is positive, but it fairly soon changes sign to produce a compression wave at the reflecting plate at time t_C. A further change takes place corresponding to time t_D and the pressure subsequently settles to a steady value p_E until time t_E. It may be noticed from figure 18 that $p_E \gtrless p_A$. According to Chisnell (loc. cit.) p_E would be equal to p_A when the shock tube is operated in the 'tailored interface' mode (no net reflection from the contact region) (see Hertzberg et al, 1955), $p_E < p_A$ for shock strengths below that for 'tailoring' and $p_E > p_A$ in the 'over-tailored' condition. Thus the tailored-interface mode corresponds to $W(X_m) \approx 5.3$. Allowing for attenuation of the shock wave as it proceeds along the shock tube, this corresponds to a shock Mach number of about 6.3 at the diaphragm, and it is conditions at the diaphragm which determine the energy ratio across the contact region. The value 6.3 is the ideal theoretical value for tailoring of the present shock tube using hydrogen to drive shocks into nitrogen.

When the time of arrival of the first disturbance from the interaction of the reflected shock with the front of the contact region is estimated*, the curve labelled t_5 in figure 20 is obtained. It is seen that t_5 corresponds fairly closely with t_B (or t_C)+. The time t_E at which the

---

* For this calculation the contact region is assumed to be travelling with the same velocity as the incident shock, since many observers have found that at about 120 tube diameters from the diaphragm the duration of the hot flow in region 2 remains fairly constant along the tube. The position of the front of the contact region is obtained from the measurements made behind the incident shock front (see Section 3). The wave reflected from the interaction is assumed to travel at the local acoustic speed a_5.

+ The initial disturbance at t_B may correspond to some other interaction, for example, between the reflected shock and boundary layer transition.

further fall in pressure begins corresponds reasonably well with the expected time of arrival of the reflected head R_H of the rarefaction wave generated at diaphragm rupture (see figure 20).

A corresponding interpretation of the temperature records may be made, allowing for the displacement of the temperature measuring station from the end plate. The calculated time of arrival t_5 of the first wave corresponds moderately well with t_c. There would seem, however, to be no period of constant temperature corresponding to the steady pressure p_E. The gas appears to cool rapidly after time t_d and tailoring so far as the temperature is concerned does not appear to occur. This rapid cooling may result from the interaction between the reflected shock and the boundary layer, when cold gas 'leaks' along the walls of the shock tube into the hot region producing a significant effect on the measured temperature. The central core region of the flow may, however, remain hot and usable as a test sample, but this has yet to be determined.

4.2 Measurements at the entrance to a nozzle

A reflected shock tunnel relies for its operation upon the region of high temperature and pressure formed behind the reflected shock, a convergent-divergent nozzle replacing the end plate of the shock tube. The hot stagnant gas acts as the reservoir for a conventional, intermittent, blow-down supersonic tunnel.

Usually in shock-tunnels a secondary diaphragm is used, in the region of the nozzle throat, to support an initial pressure difference between the shock-tube and the expanded test-section. This is to aid the nozzle starting process and has only a small effect on the stagnation region provided the ratio of throat cross-section to shock tube cross-section is small. Again the outflow which takes place through the nozzle should have only a small effect on the wave system in the reflected shock region.

In order to ascertain just what effect the presence of a nozzle does have on the constancy of conditions in the reservoir, measurements were made just upstream of a two-dimensional nozzle, the dimensions of which are shown in figure 4. Only temperature measurements were made, at station n, the pressures measured at the reflecting plate and reported in the preceding sub-section being regarded as sufficiently representative.

Typical oscillograms and some derived temperature variations are

shown in figure 22 together with some pressure variations at the reflecting plate obtained under closely similar conditions. Points C, D and G are defined corresponding to those discussed in Section 4.1. The points C and D should correspond fairly closely with similarly labelled points on the pressure records since there is little displacement now between the measuring stations.

The temperatures are shown as functions of shock Mach number at the nozzle in figures 23. The temperature T_C corresponds much more closely with the theoretical temperature T_5 behind the reflected shock than it did in the measurements reported in Section 4.1. The discrepancy there was explained by the displacement of the measuring station from the reflecting wall, so that the reflected shock had to process gas in which a temperature gradient was known to exist. Because station n in these nozzle experiments was so much closer to the reflecting wall, this effect does not occur. Again, waves which presumably arise from the interaction of the reflected shock with the contact region produce temperature variations up to a maximum T_D which is some 200 K above T_C. The times of arrival are shown in figure 24 as functions of shock Mach number at the nozzle. The time t_C accords well with that obtained from the pressure measurements. However, the gas begins to cool (at time t_D) somewhat earlier than the pressure began to fall. Three possible causes suggest themselves:

1. Heat transfer takes place to the cold wall of the nozzle close to the measuring station, so that the gas is cooled.
2. Outflow through the nozzle causes an expansion to travel into the reservoir, thereby causing the temperature to fall.
3. Cold gas 'leaks' along the wall as a result of shock-boundary layer interaction thereby depressing the measured temperature.

Of these, the last is probably the most significant. Heat transfer to the nozzle wall should also affect T_C so that it is less than T_5, and there is no evidence of this. Again an expansion wave would move rapidly in the hot gas and there is no reason why its effects should be delayed until time t_D. However the leakage of cold gas, blamed earlier for the fall in temperature, may well have a more severe effect close to the reflecting wall or nozzle entrance, because this cold gas as it travels

forward is being forced in towards the centre of the tube by the presence of the end wall, and so it tends to collect near the measuring station. If this explanation is justified, one is forced to conclude that small shock tubes, such as the one used here, have severe limitations when used to generate the reservoir gas for driving a hypersonic nozzle.

Finally the data, with some extrapolation outside the Mach number range in which measurements could be made, are re-presented in figures 25 and 26 by way of a "calibration" for this shock-tube. They provide a reasonable estimate of the temperature variation and the duration of hot flow at the entrance to the nozzle. The variations in pressure are assumed to be adequately represented by the measurements made at the reflecting plate and described in Section 4.1.

5. Concluding remarks

A 'calibration' has been presented for the Queen Mary College 38.1 mm square channel shock tube when it is used with hydrogen to drive shocks into nitrogen, both gases being at room temperature initially. Detailed temperature and pressure measurements made behind the incident shock and in the reflected shock region, including some measurements at the entrance to a convergent-divergent nozzle, have been reported. The incident shock Mach number ranged from about 3.5 to 7. The measurements show clearly that for a shock tube of these dimensions, real gas effects play a very important part in determining the state of the shocked gas.

Behind the incident shock front a temperature rise of some 200 K occurs over the hot flow duration. The latter is considerably shorter than predicted by ideal, imperfect gas theory, as has been found by many other investigators. The pressure in this region was found to remain constant during the hot flow duration at a value which agrees well with ideal theory, but a marked pressure gradient which appeared after the arrival of cooler gas remains unexplained.

Vibrational energy relaxation times obtained from the incident shock measurements are in reasonable agreement with results obtained by other workers.

Except for the region very close to the reflecting wall, ideal imperfect gas theory is unable to explain the varying conditions observed behind the reflected shock. Although the ideal theory accounts well for the magnitude of the pressure and temperature just after shock reflection, temperatures measured 25.4 mm (that is, less than one tube hydraulic diameter) from the reflecting surface were found to be significantly higher than those predicted. This has been explained as a magnification

by the reflected shock of the temperature gradient observed behind the incident shock.

The achievement of a tailored-interface condition does not seem practical for a shock-tube of these dimensions, in which viscous effects and contact surface mixing play a dominant role.

When a shock tube is to be used to drive a hypersonic nozzle, attention during design should be concentrated on producing rapid diaphragm rupture, so that the contact region is not too extensive, and a minimum of shock attenuation. Because viscous effects and interface mixing may prevent the tailored-interface condition from being achieved it would seem advisable to choose the length of the shock tube according to the testing time required and then to make the cross-sectional dimensions as large as practical considerations, such as strength, manufacture and costs, will allow, thereby diminishing shock attenuation, and the appearance of severe temperature gradients in the shock-processed gas.

Acknowledgements

This work was supported by the then Ministry of Technology under an extra-mural agreement, and one of us (M.J.L.) would like to express his gratitude for a maintenance grant during the course of the project of which this forms a part.

Nomenclature

a_i	speed of sound in region i
p	pressure
p_i	pressure in region i (see suffices)
p_J	measured pressure at point J (see suffices)
P_{ij}	pressure ratio p_i/p_J
t	trace (real) time
t_i	duration of region i (see suffices)
t_p	particle time
t_J	time to point J (see suffices)
T	active mode temperature
T_i	equilibrium imperfect gas temperature in region i (see suffices)
T_v	vibrational temperature
T_J	measured temperature at point J (see suffices)
T_L	lamp brightness temperature
W(X)	incident shock Mach number at X
X	distance from main diaphragm station
X_a	distance from diaphragm station to station a (see suffices)
α	$(\gamma+1)/(\gamma-1)$
β	$(\gamma-1)/2\gamma$
γ	ratio of principal specific heat-capacities
τ_N	relaxation or napier time, μs atm.

Suffices

a	channel stations: a = i, j, k, l, m, n
i	1, 2, 3 etc.
J	1, 2, 3 etc.
J	points on measured data: J = A, B, C, D, E, H, S OR c, d, f, g, l

Abbreviations

C		contact surface
R_H		reflected head of rarefaction wave
R_T		tail of rarefaction wave
S		shock wave
?		Mach wave
	OR	shock wave
	OR	rarefaction wave

References

Ackroyd, J.A.D., 1964 Ph.D. Thesis, University of London.

Allen, J.W., 1968 'An Experimental Study of the Interaction between the Reflected Shock Wave and a Turbulent Boundary Layer in a Shock Tube' - R.A.E. Tech. Rep. 68089.

Bernstein, L., and Goodchild, R.O. 1967 'High Sensitivity Piezoelectric Transducer for Wave Velocity Measurements in Shock-Tubes' - Rev. Sci. Instr. 38, p.971.

Bernstein, L. 1963a 'Some Measurements of Shock-Wave Attenuation in Channels of Various Cross-Sections' - R. & M. No.3321.

Bernstein, L. 1963b 'Tabulated Solutions of the Equilibrium Gas Properties behind the Incident and Reflected Normal Shock Wave in a Shock Tube' - A.R.C., C.P. No. 626.

Chisnell, R.F. 1955 'The Normal Motion of a Shock Wave through a Non-Uniform One-Dimensional Medium' - Proc. Roy. Soc. A232.

Davies, L. 1965 'The Interaction of the Reflected Shock with the Boundary Layer in a Shock Tube and its Influence on the Duration of Hot Flow in the Reflected-Shock Tube' -

Part I , N.P.L. Aero Rep. 1158.
Part II, N.P.L. Aero Rep. 1167.

Gaydon, A.G. and Hurle, I.R. 1963 'The Shock Tube in High Temperature Chemical Physics' - Reinhold Publ. Co., N.Y.

Glass, I.I. and Hall, J. 1959 'Shock Tubes' - Handbook of Supersonic Aerodynamics, NAVORD Rep. 1488 (Vol.6), Section 18.

Hertzberg, A., Smith, W.E., Glick, H.S., Squire, W. 1955 'Modifications of the Shock-Tube for the Generation Hypersonic Flow' - Cornell Aero. Lab. Report CAL AD/789/A/2

Holbeche, T.A. and Spence, D.A. 1964 'Theoretical and Experimental Investigation of Temperature Variation behind Attenuating Shock Waves' - Proc. Roy. Soc. A279, p.111.

Hooker, W.J. 1961 'Testing Time and Contact-Zone Phenomena in Shock Tube Flows' - Phys. Fl. 4, pp.1451-1463.

Huber, P.W. and Kantrowitz, A. 1947 'Heat Capacity Lag Measurements in Various Gases' - Journ. Chem. Phys. 15, p.275.

Johanneson, N.H. 1961 'Analysis of Vibrational Relaxation Region by Means of the Rayleigh-Line Method' - Journ. of Fluid Mechanics, 10, p.25.

Lewis, M.J., Teague, M.J., Malcolme-Lawes, D.J., and Bernstein, L.	1969	'Production of Free Sodium Atoms for the Spectrum Line Reversal Technique' - A.I.A.A. J., 7, p.1798.
Mirels, H.	1971	'Boundary Layer Growth Effects in Shock Tubes' - Proc. 8th Int. Shock Tube Symp., London.
Rudinger, G.	1961	'Effect of Boundary Layer Growth in a Shock Tube on Shock Reflection from a Closed End' - Phys. Fl. 4, p.1463.
Russo, A.L., and Watt, W.S.	1968	'Infrared Measurements of the Vibrational Excitation and De-Excitation Rates of N_2 using CO Additive' - Cornell Aero. Lab. Rep. AF-2567-A-1.
Sebacher, D.I.	1967	'A Correlation of N_2 Vibrational to Translational Relaxation Times' - A.I.A.A. Journal, 5, p.819.
Simpson, C.J.S.M., Chandler, T.R.D. and Bridgeman, K.B.	1967	'Effect on Shock Trajectory of the Opening Time of Diaphragms in a Shock Tube' - Phys. Fl. 10, p.1894.
Spence, D.A.	1961	'Unsteady Shock Propagation in Relaxing Gases' - Proc. Roy. Soc. A 264, p.221.
Teague, M.J.	1968	Ph.D. Thesis, University of London.
Wittliff, C.E. and Wilson, M.R.	1967	'Shock Tube Driver Techniques and Attenuation Measurements' - Cornell Aero. Lab. Rep. No. AD-1052-A-4.

Appendix A

Active-mode-temperature and particle-time corrections to the incident shock measurements

Ideally the temperature behind the incident shock is constant up to the contact surface. Ignoring relaxation phenomena, shock attenuation gives rise to a temperature gradient; the temperature seen by a fixed observer appears to increase as the shocked gas flows past. This rise in temperature is due to the gas having been processed by a stronger shock upstream of the measuring station compared with the gas actually shocked at this station. Particle acceleration increases the rate at which gas particles arrive at a measuring station thereby enhancing the temperature gradient. Where shock attenuation is significant in a shock tube, the temperatures of the active mode and the particle time, inferred from vibrational temperature measurements and 'trace' times, should be corrected for these real gas effects.

Following the method presented by Holbeche & Spence (1964), these corrections were obtained for the present incident shock measurements. The measurements gave the variation of T_V with t, as shown in figure 6, together with the hot flow duration. The gas velocity at m was assumed to be a linear function of t over the hot flow duration. Its initial value was determined from imperfect gas information (Bernstein, 1963b) based upon $W(X_m)$. The gas velocity at the front of the contact region was assumed to be equal to $W(X_m)$. A value of 'trace' time thereby provided a gas velocity, which gave a corresponding particle time provided that the shock trajectory was known along the channel. The shock trajectory was determined from the present shock speed measurements and those presented by Bernstein (1963a). This particle time also determined the shock strength when this gas element was shocked. The active mode temperature was determined from this shock strength and the measured vibrational temperature at the chosen 'trace' time. The results of applying this extremely crude analysis to the incident shock measurements are indicated in figure 7.

Appendix B

Reflected-shock correlations

The incident shock measurements indicated that a temperature gradient was present behind the shock. The temperature measurements in the reflected shock region indicated that this gradient was magnified by the reflected shock. Furthermore, the incident shock results showed that the contact-region was much closer to the shock than predicted by ideal theory. The duration and dimensions of the hot gas in the reflected shock region will thus be much smaller than the ideal values, because the reflected shock will meet the contact-region much earlier than predicted ideally.

A simple model was used to account for the above phenomena and to provide some correlation of the experimental results with theory, at least for region 5. The time scale and hence the dimensions of region 5 were established by assuming that the reflected shock velocity was constant and equal to its imperfect gas value (Bernstein 1963b) based upon $W(X_m)$. The velocity of the contact-region was assumed to be equal to $W(X_m)$ and its initial position, relative to the reflected shock, was determined from the incident shock measurements of the hot flow duration. The reflected-shock contact-region interaction was treated very simply. The front of the contact-region was assumed to be a contact surface. The energy ratio across this surface was based upon the ideal value determined from the incident shock Mach number at the diaphragm station. This shock speed was extrapolated from the incident shock attenuation information. The wave reflected from the contact-region and its velocity were then determined from ideal theory. The time t_5 was then easily determined. The time t_5' was determined in a similar fashion but allowance was made for the displacement from the reflecting plate of the temperature measurement station. To correlate with ideal theory the measured temperature 25.4 mm from the reflecting plate, it was assumed that the temperature ratio (T_5/T_2) across the reflected shock was constant. The measured variation of T_2 thereby provided the variation of T_5.

The results of the above correlations are presented in figures 19 to 21.

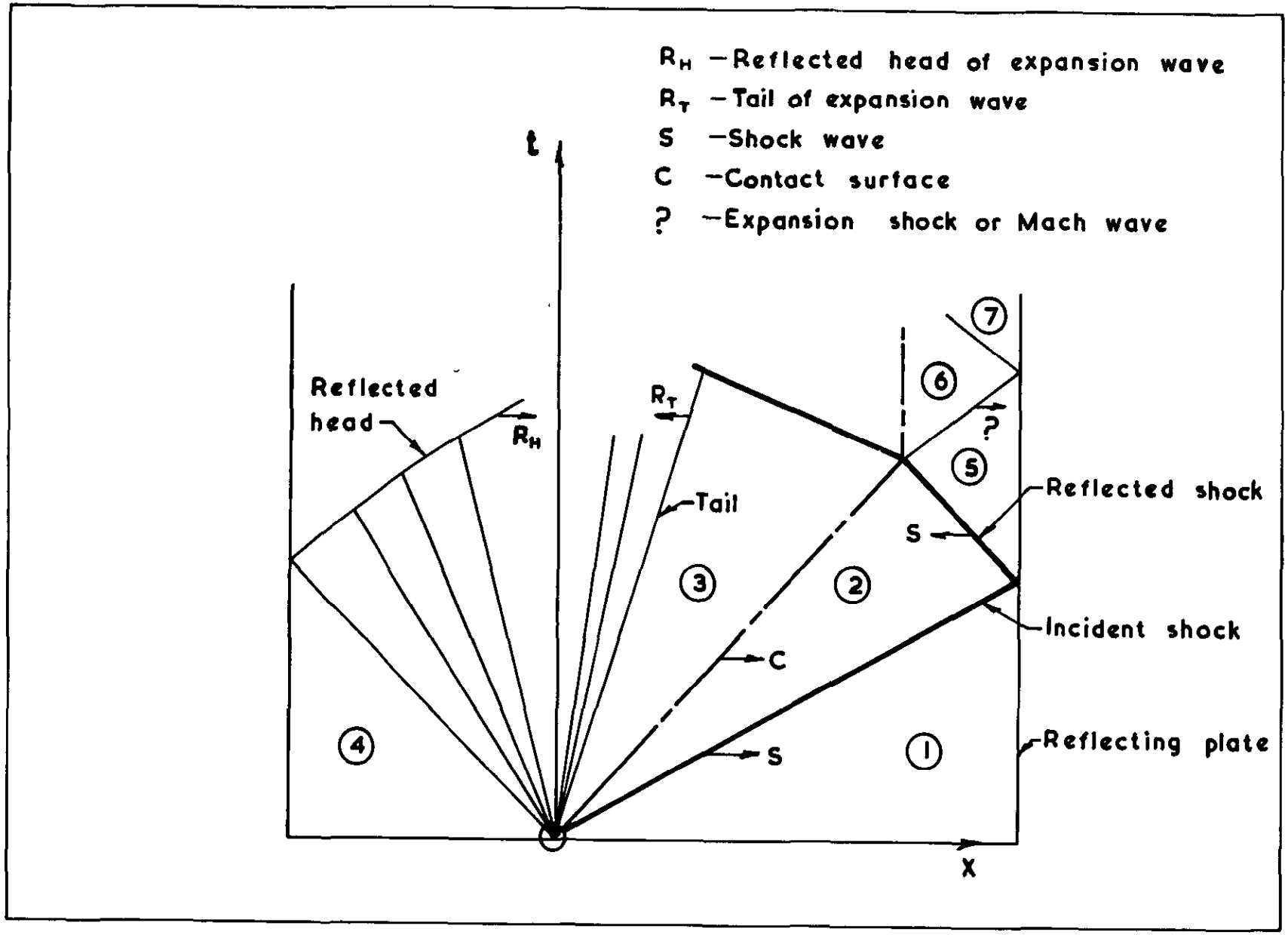

Figure 1 Ideal behaviour of the shock system in a shock tube

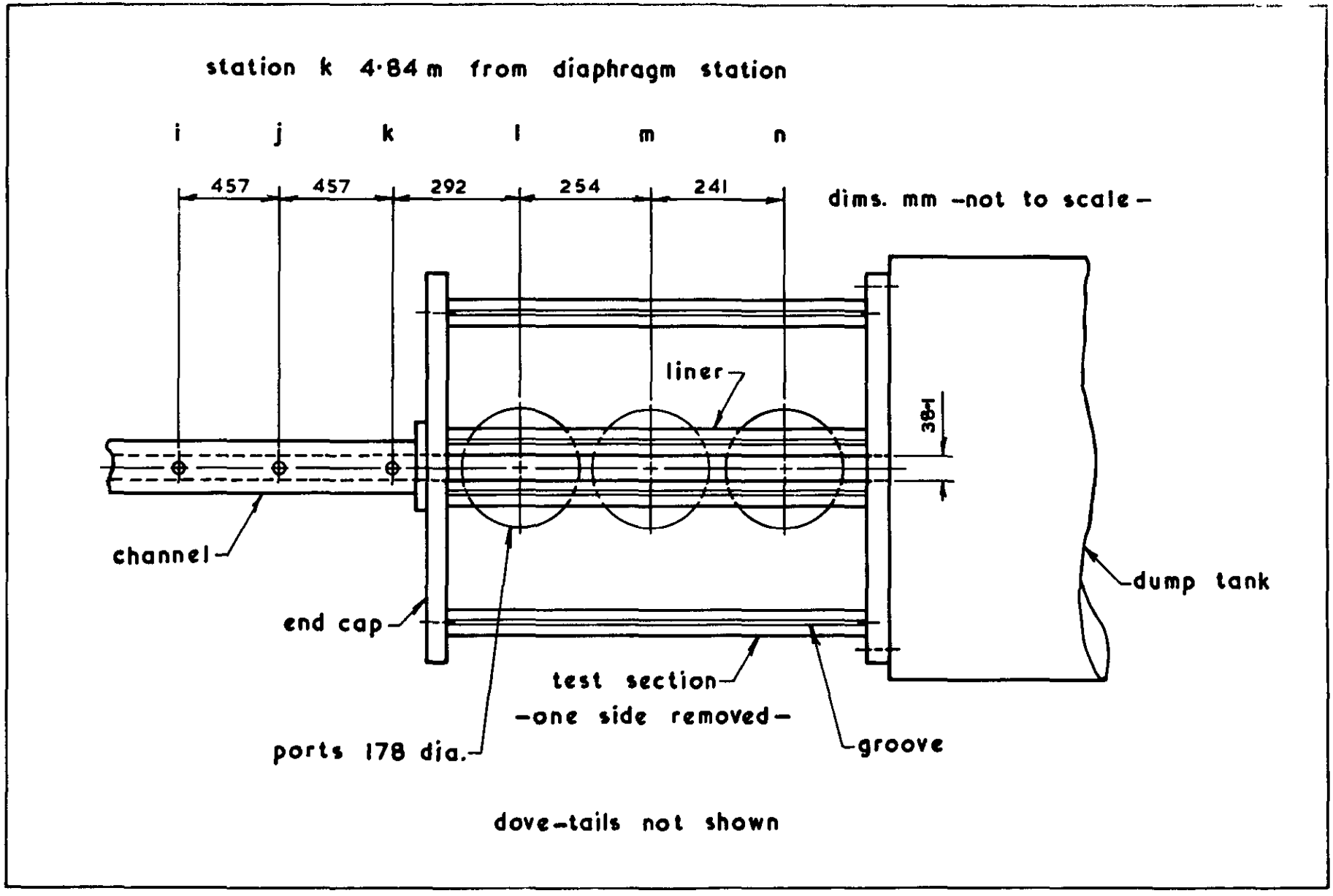

Figure 2 **Test section**

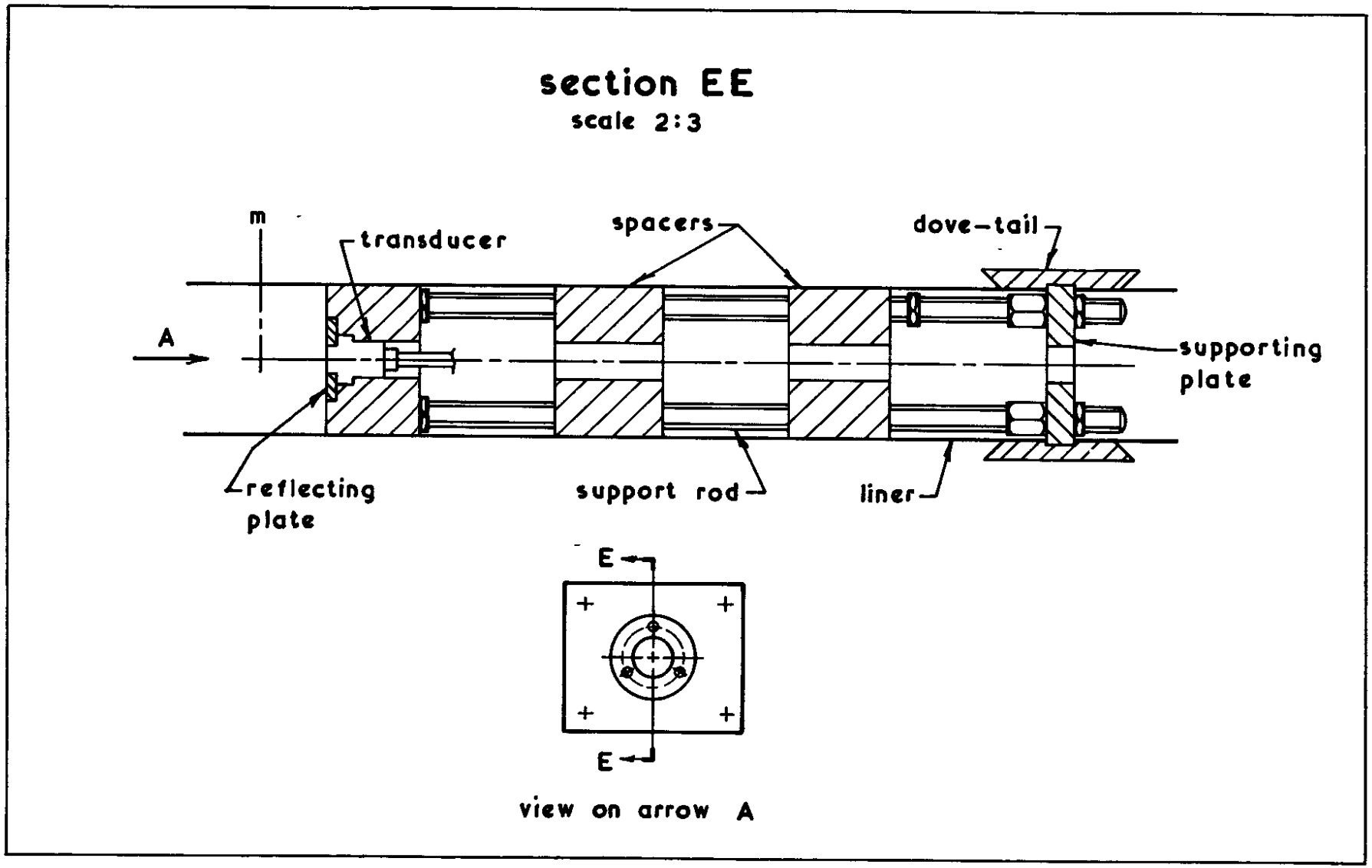

Figure 3 Reflecting plate assembly

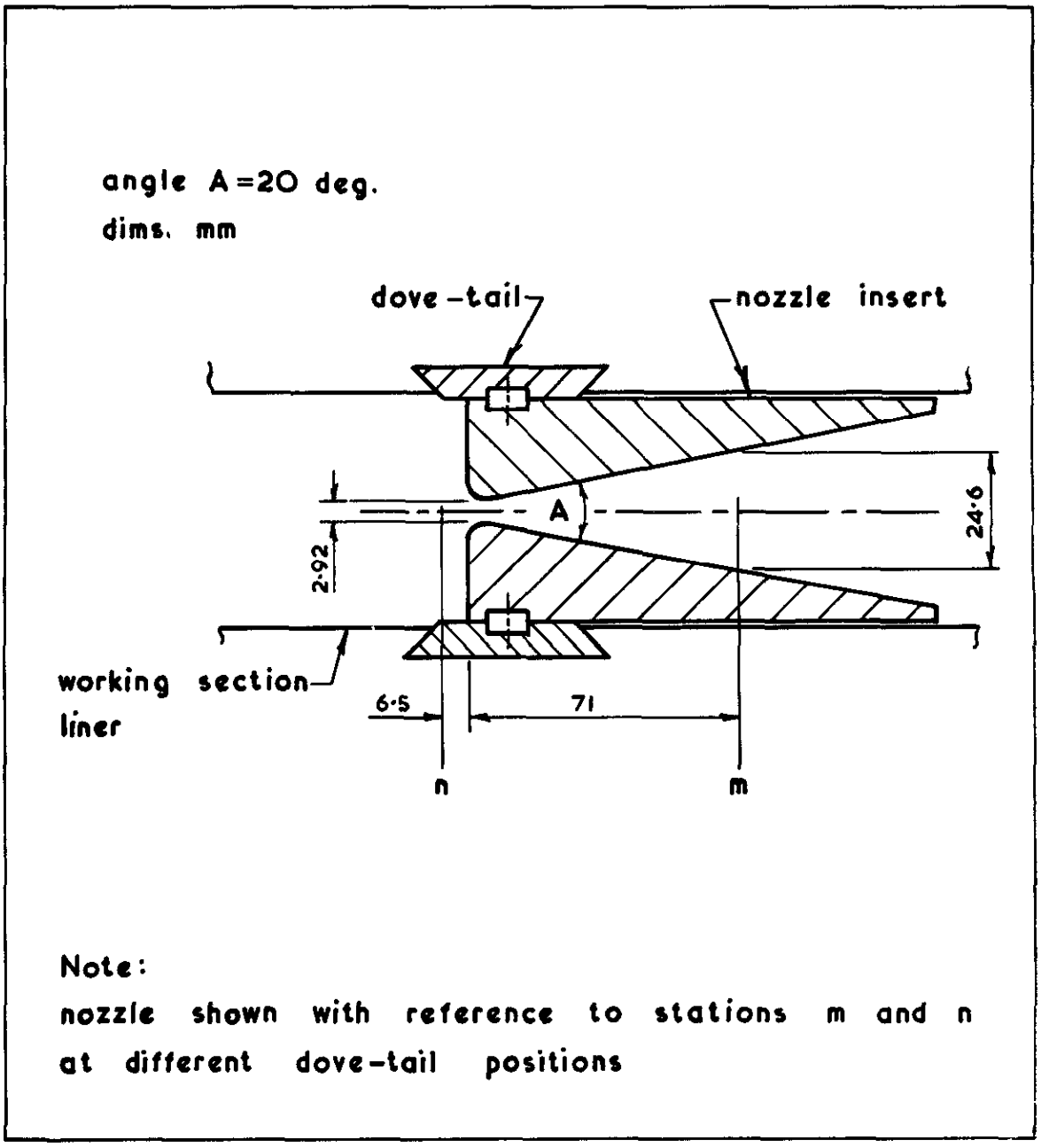

Figure 4 **The two-dimensional nozzle**

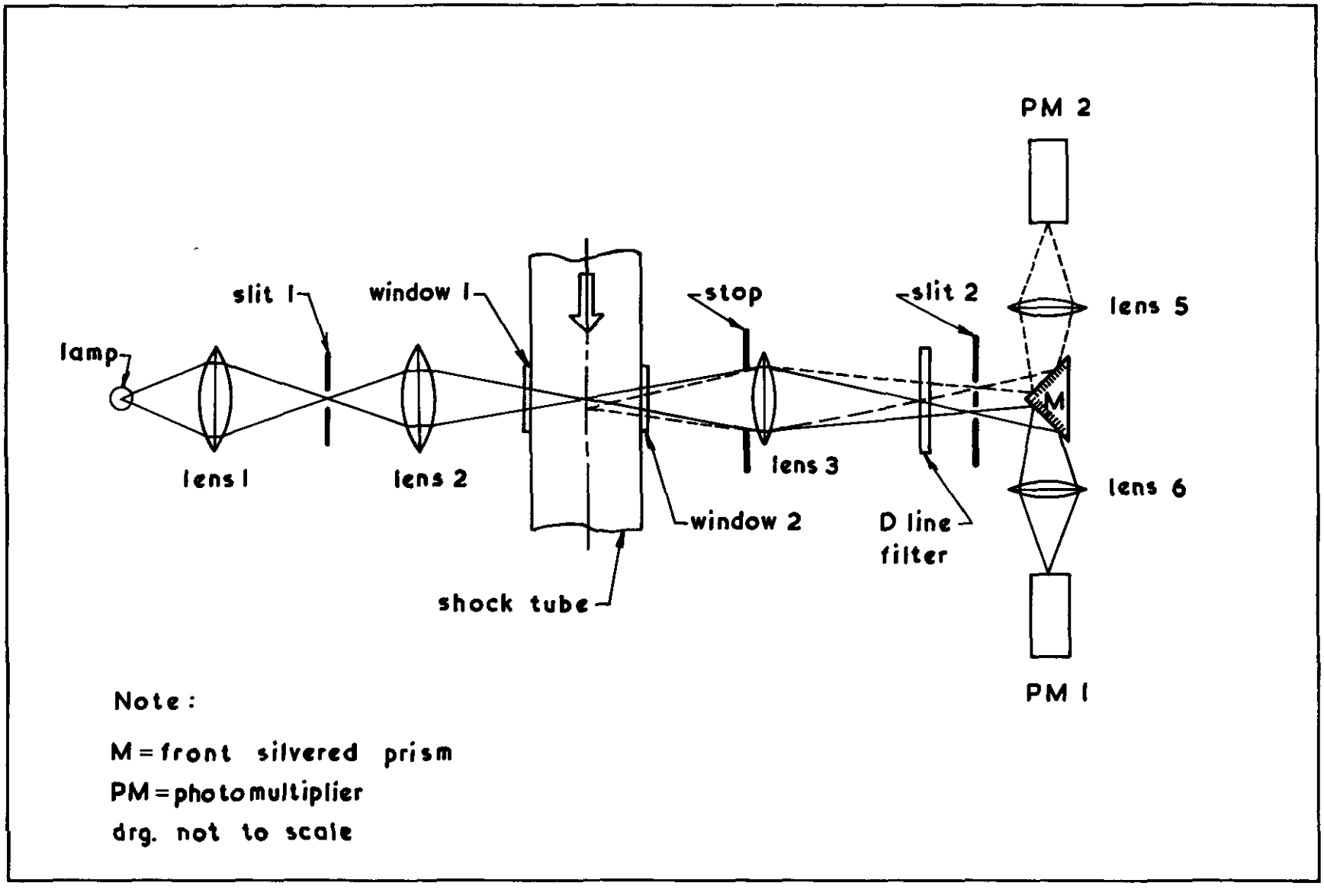

Figure 5 **The optical system**

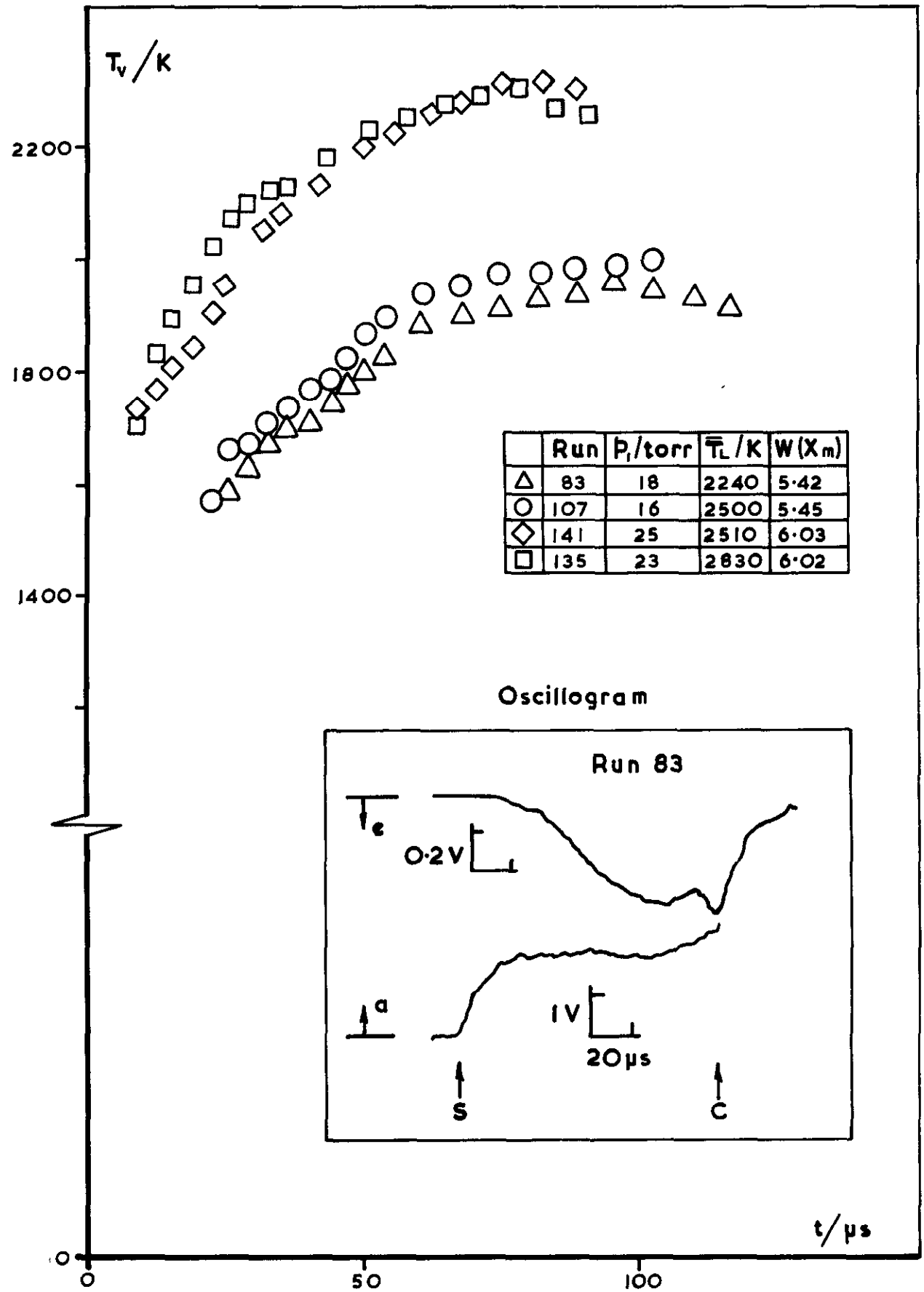

Figure 6 Vibrational temperature variation
-shock excitation-

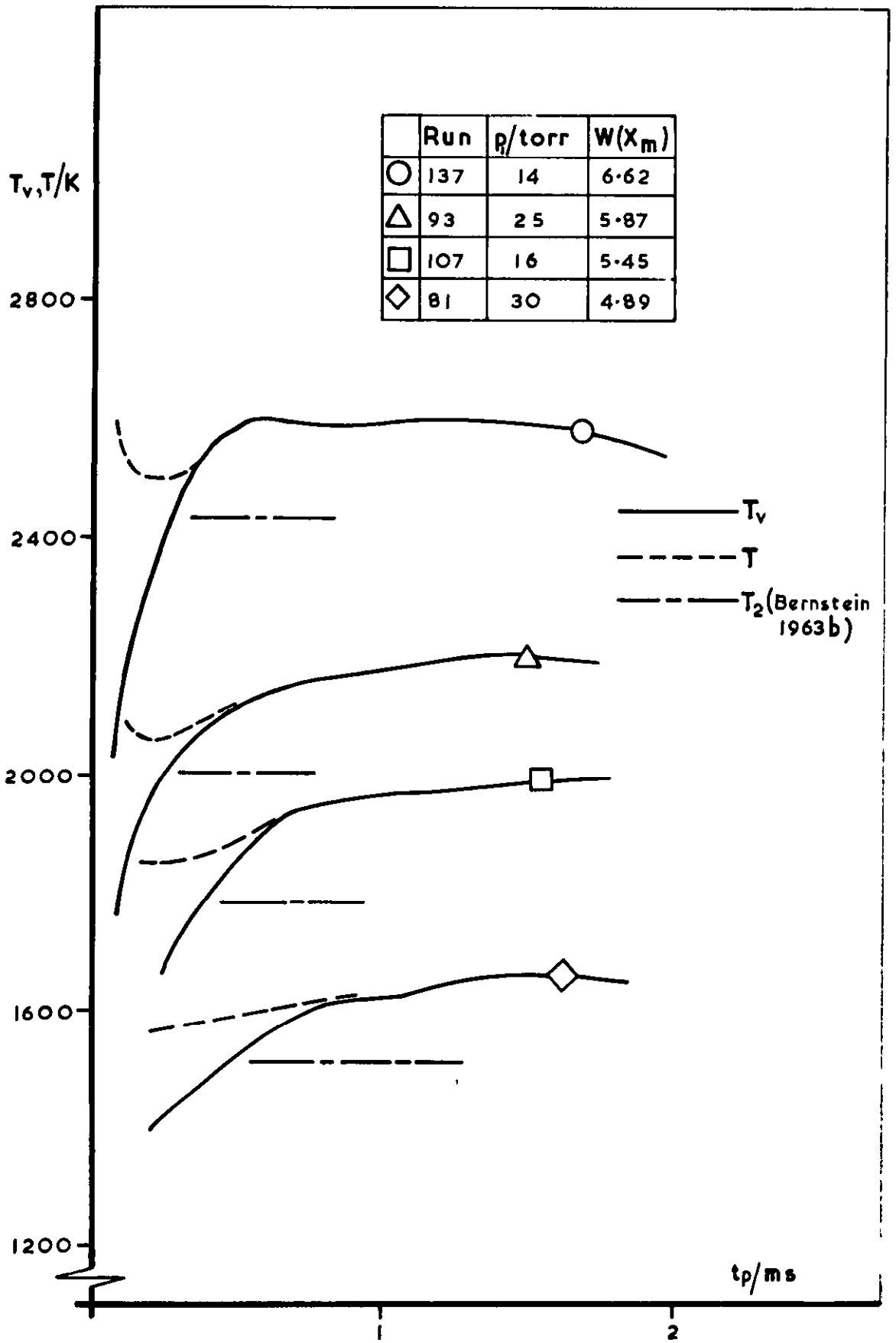

Figure 7 Temperature variation behind incident shock

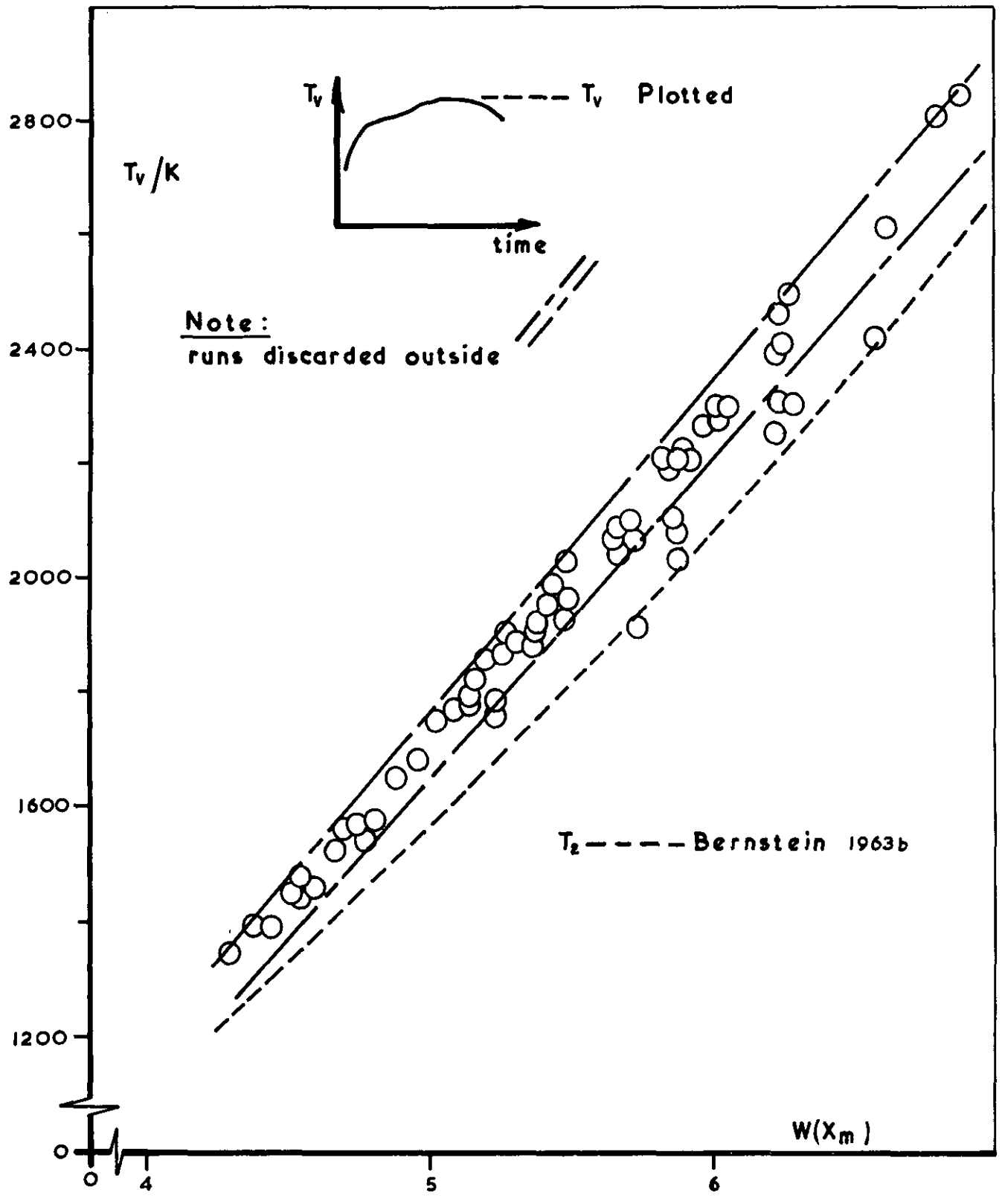

Figure 8 Temperature gradients in the flow and eligibility of data

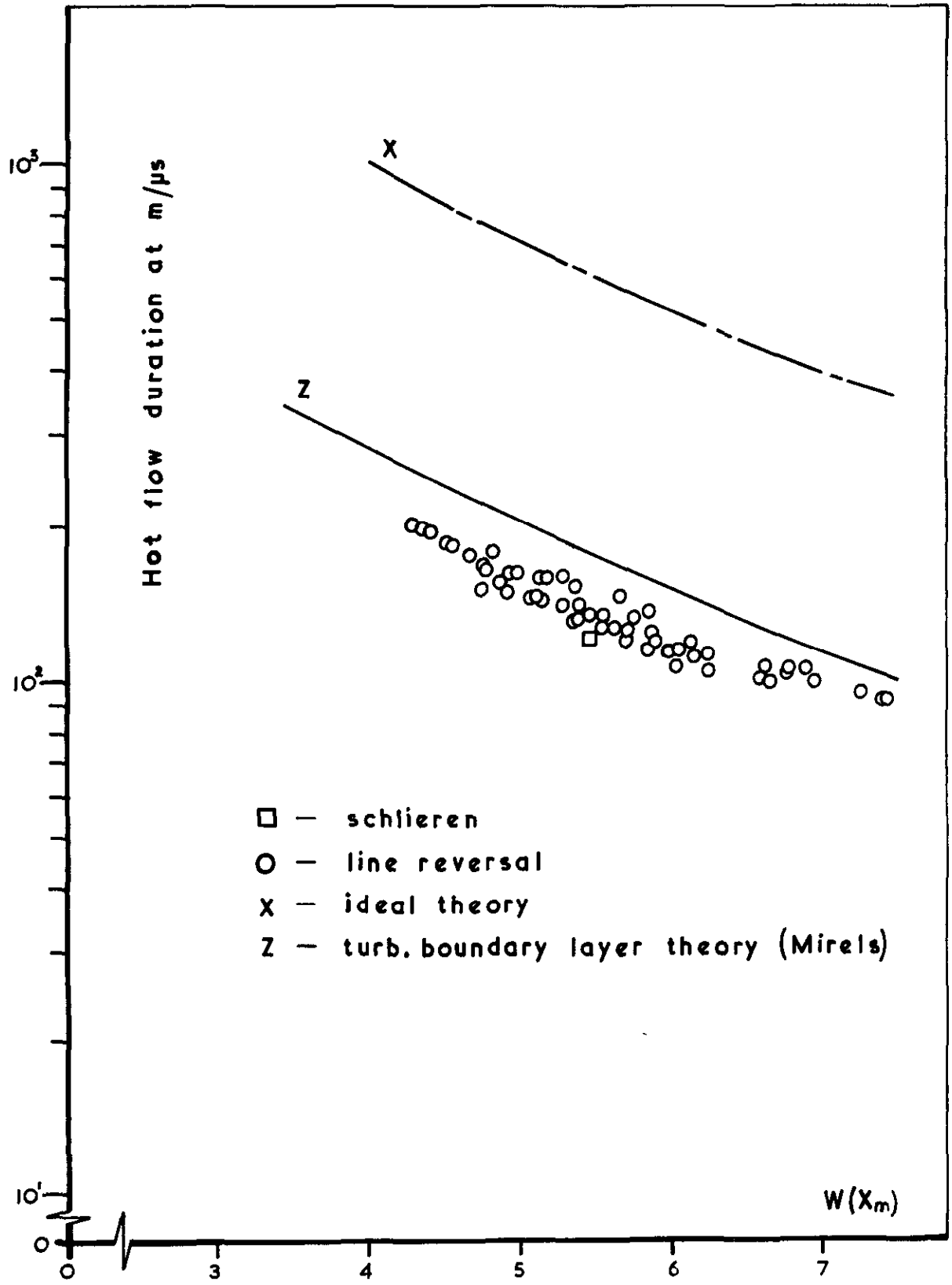

Figure 9 **Hot flow duration**
–behind incident shock–

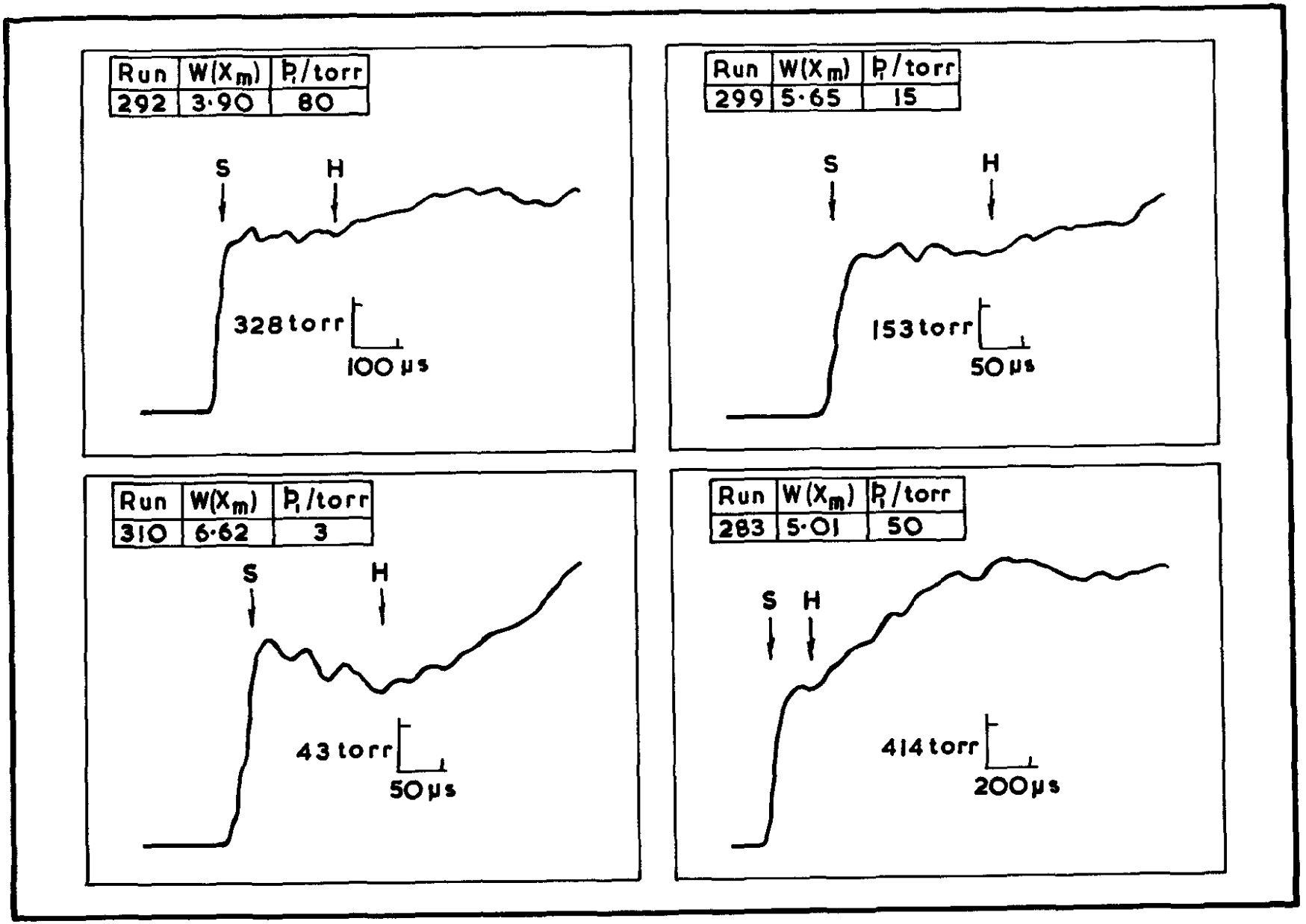

Figure 10 **Static pressure variation behind a shock wave**

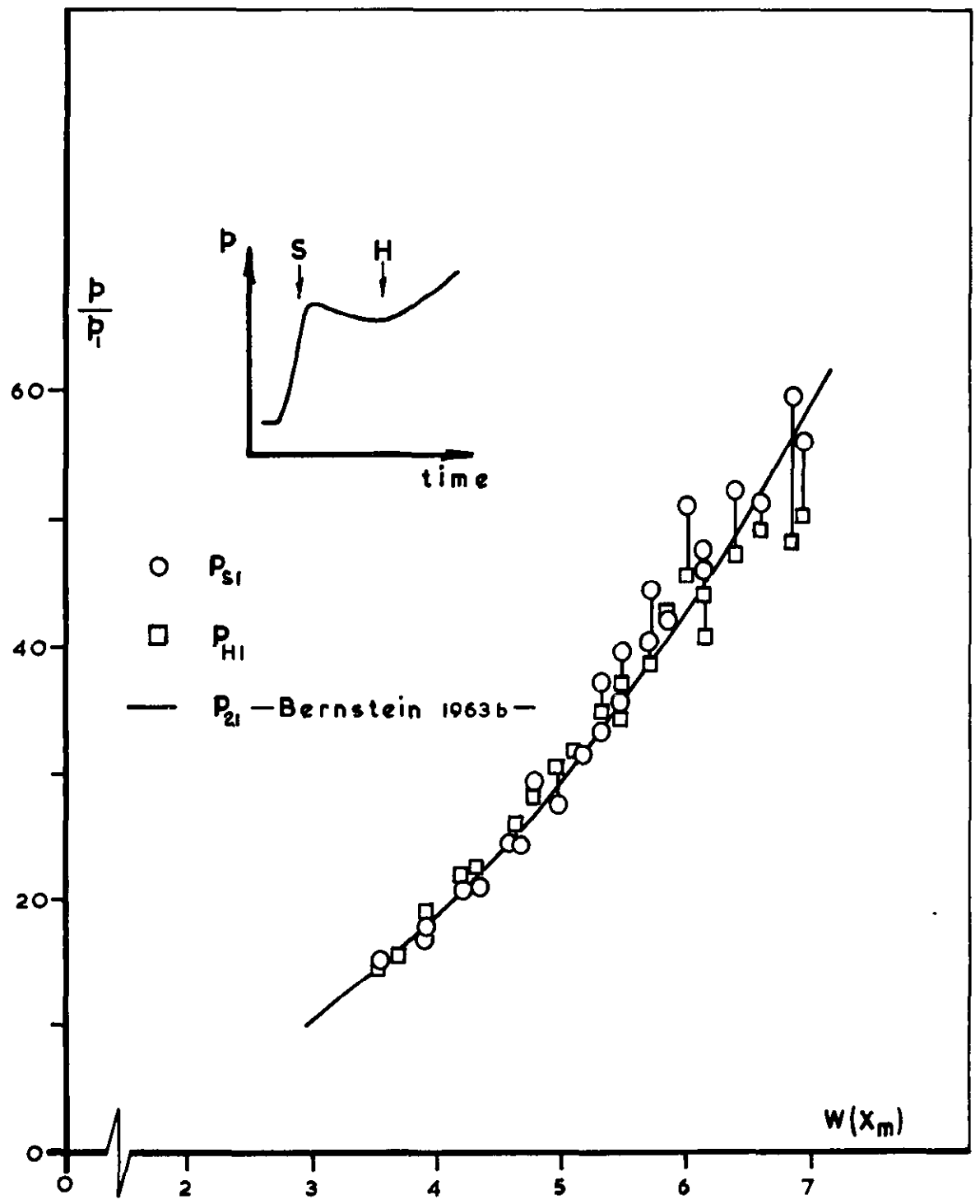

Figure 11 **Pressure behind shock wave**

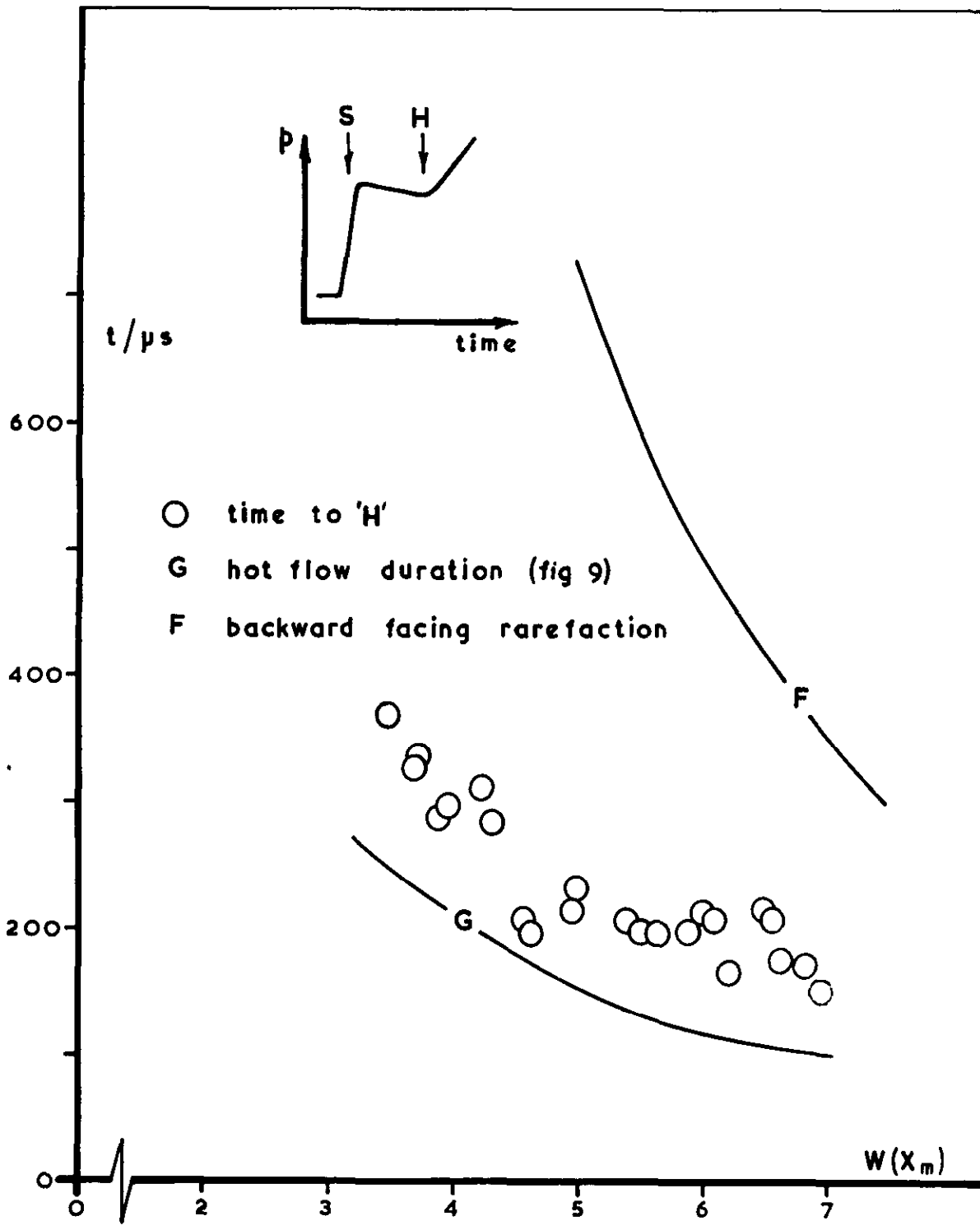

Figure 12 **Steady pressure duration behind incident shock**

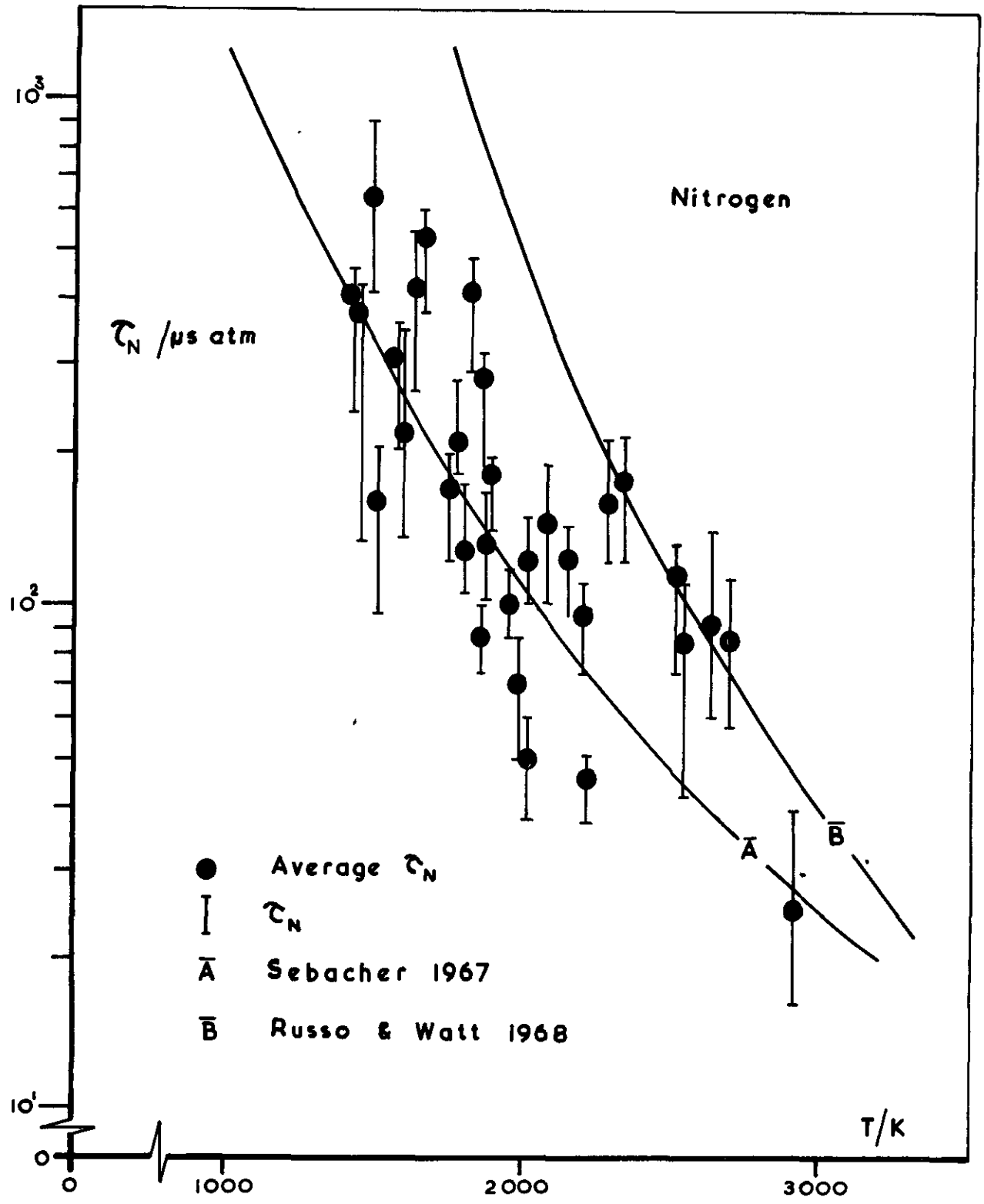

Figure 13 **Shock excitation relaxation rates**

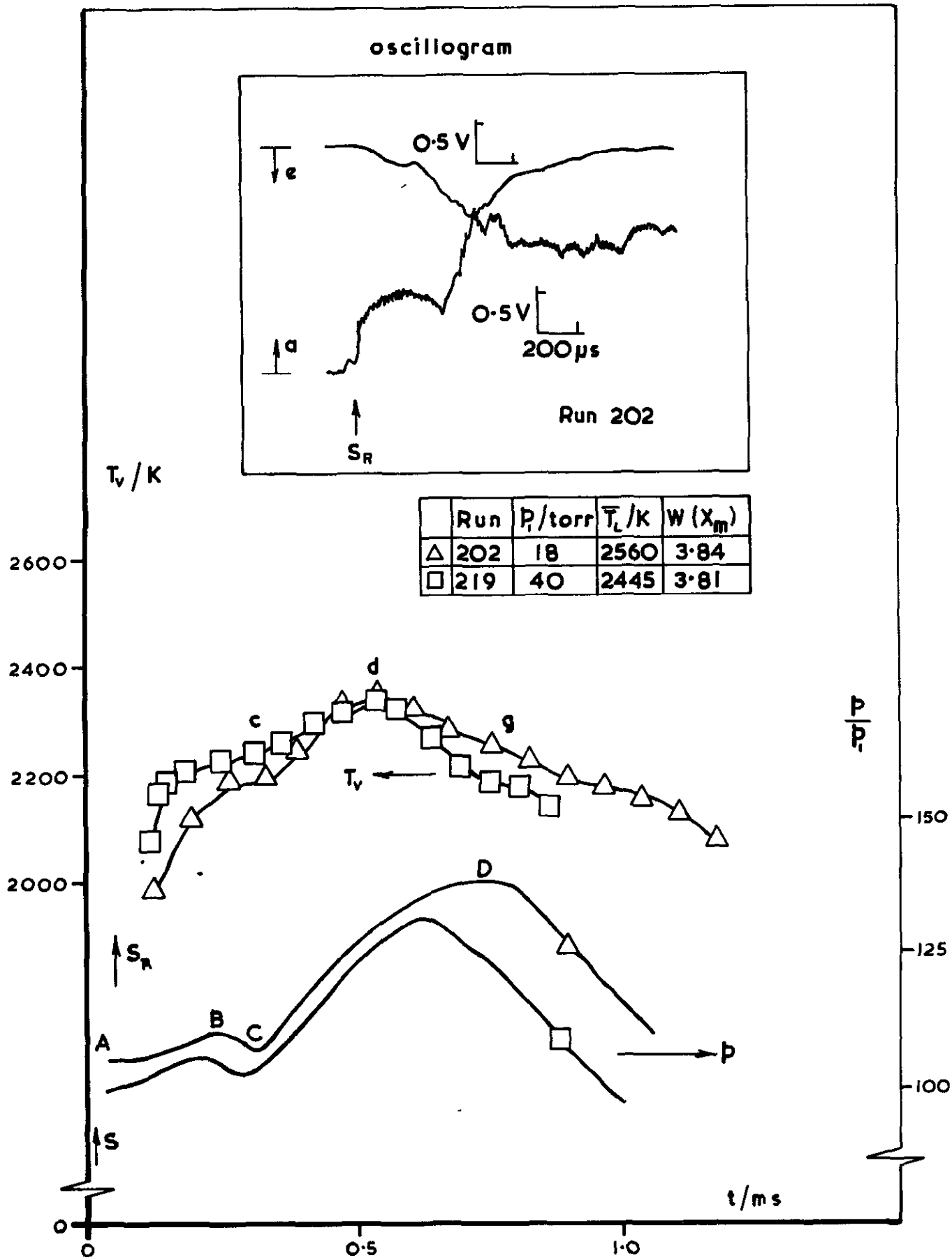

Figure 14 **Temperature and pressure variations — reflected shock region —**

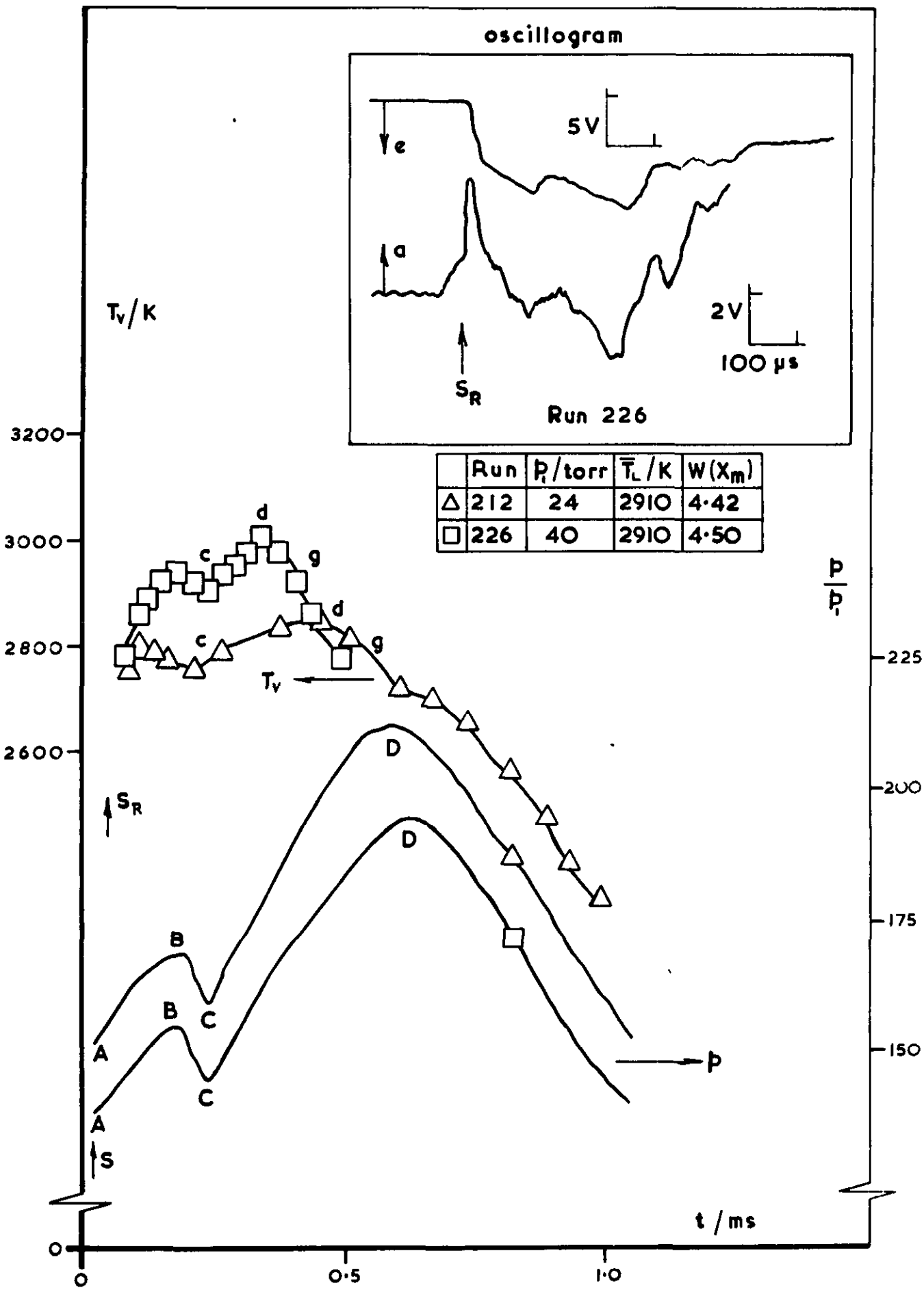

	Run	p_1/torr	$\bar{T}_L$/K	W(X_m)
△	212	24	2910	4·42
□	226	40	2910	4·50

Figure 15 **Temperature and pressure variations — reflected shock region —**

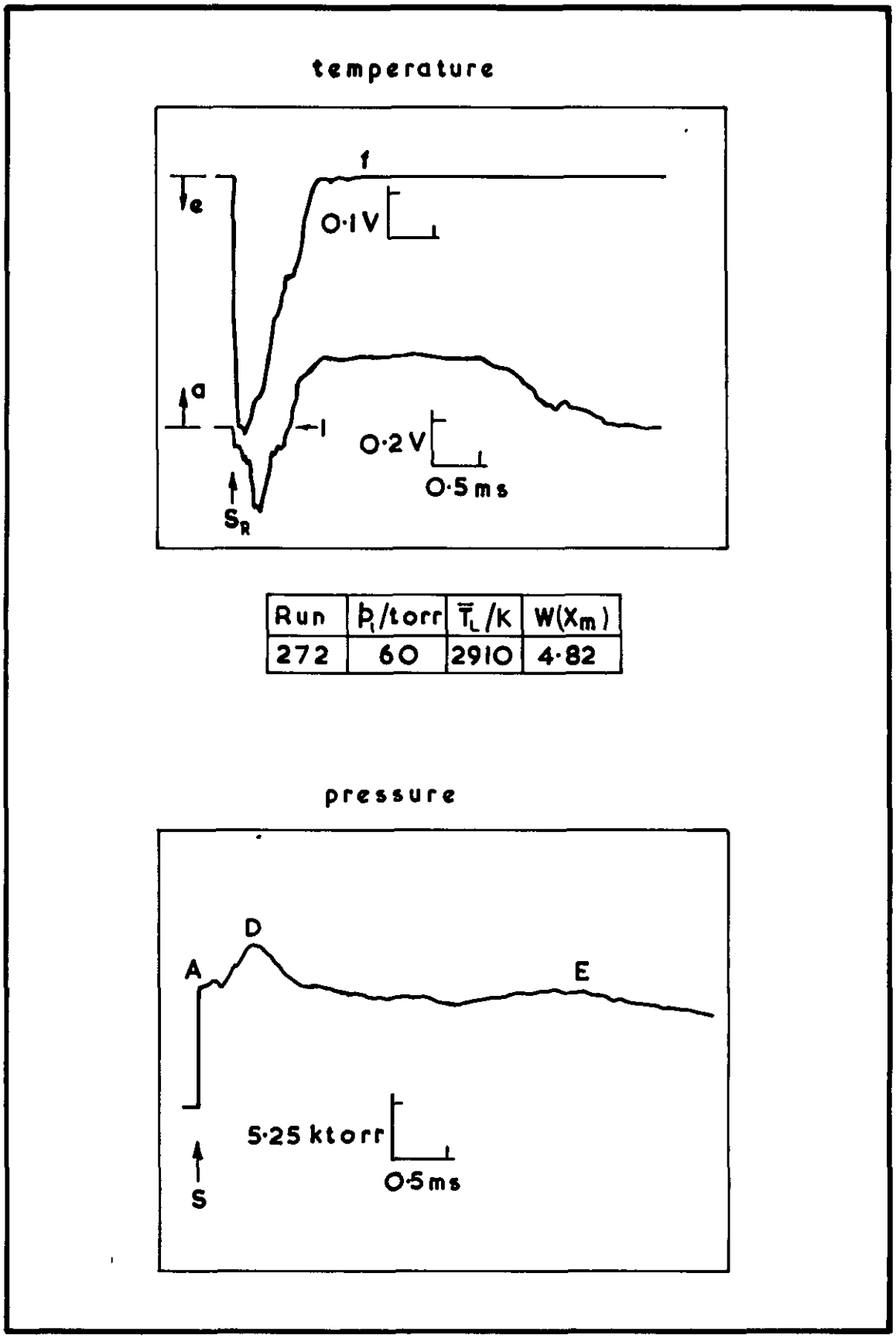

Run	$\bar{p}_1$/torr	$\bar{T}_L$/K	W(X_m)
272	60	2910	4·82

Figure 16 'Long time' oscillograms
–reflected shock region–

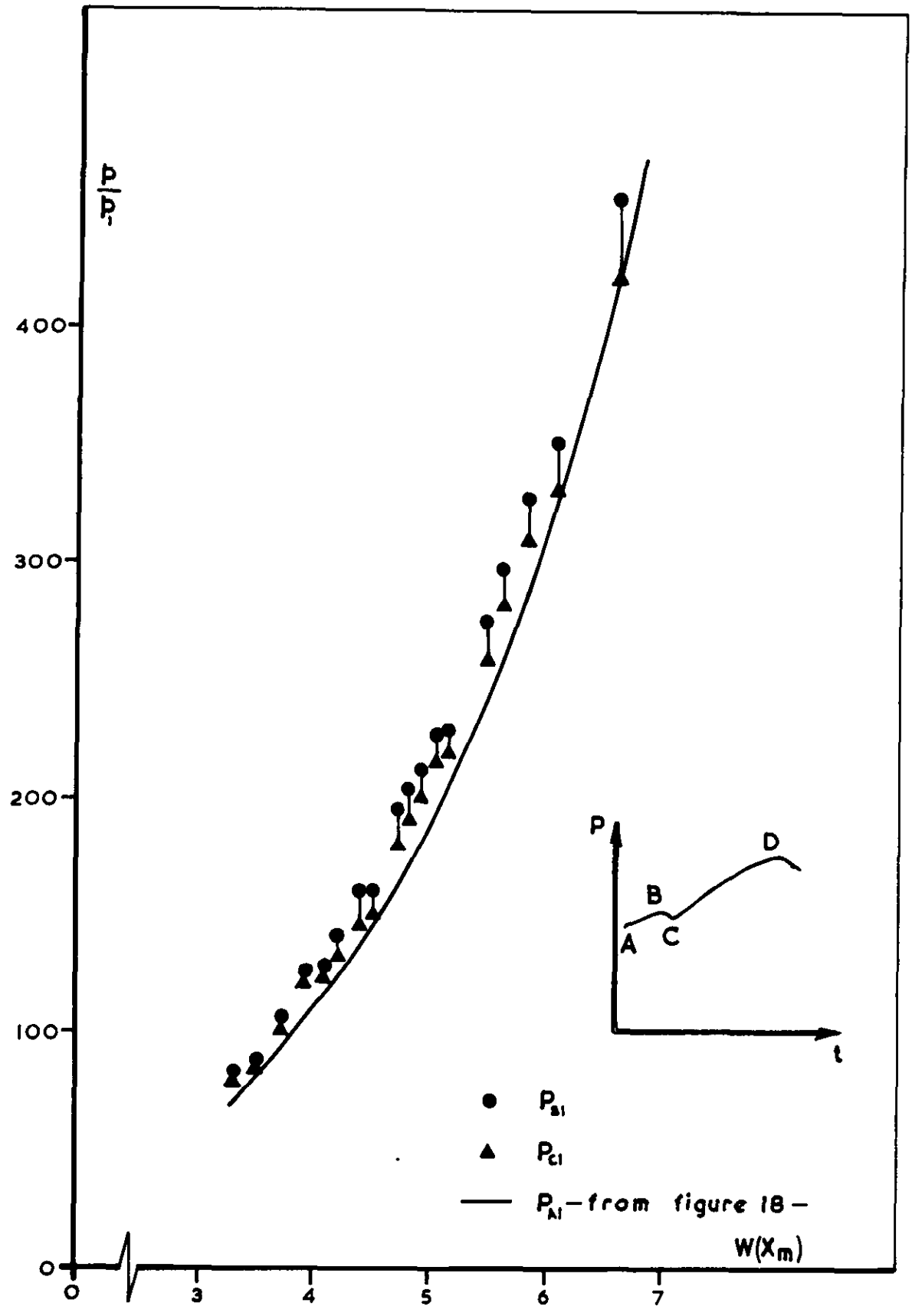

Figure 17 Pressure variation at reflecting plate

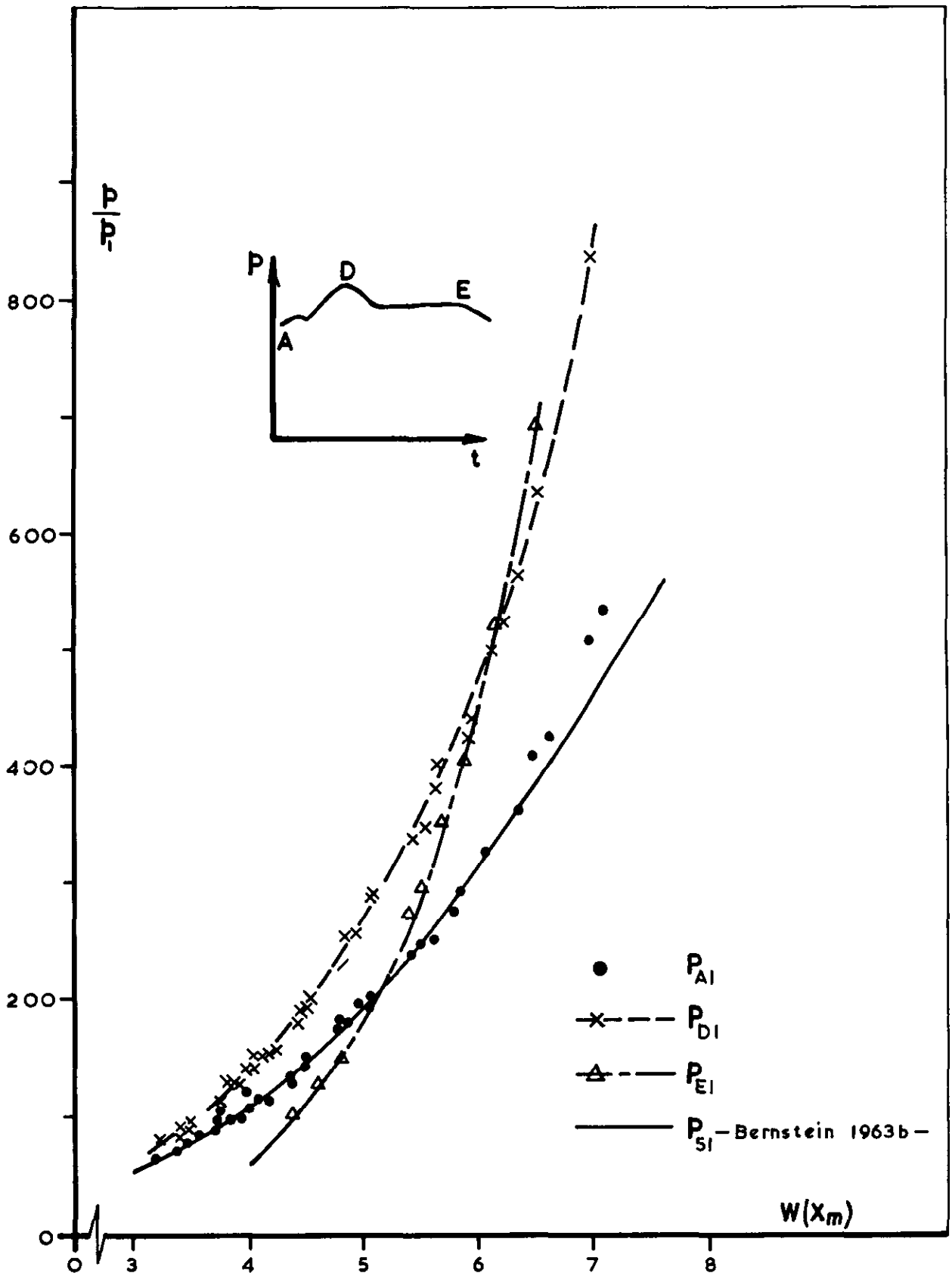

Figure 18 Pressure variation at reflecting plate

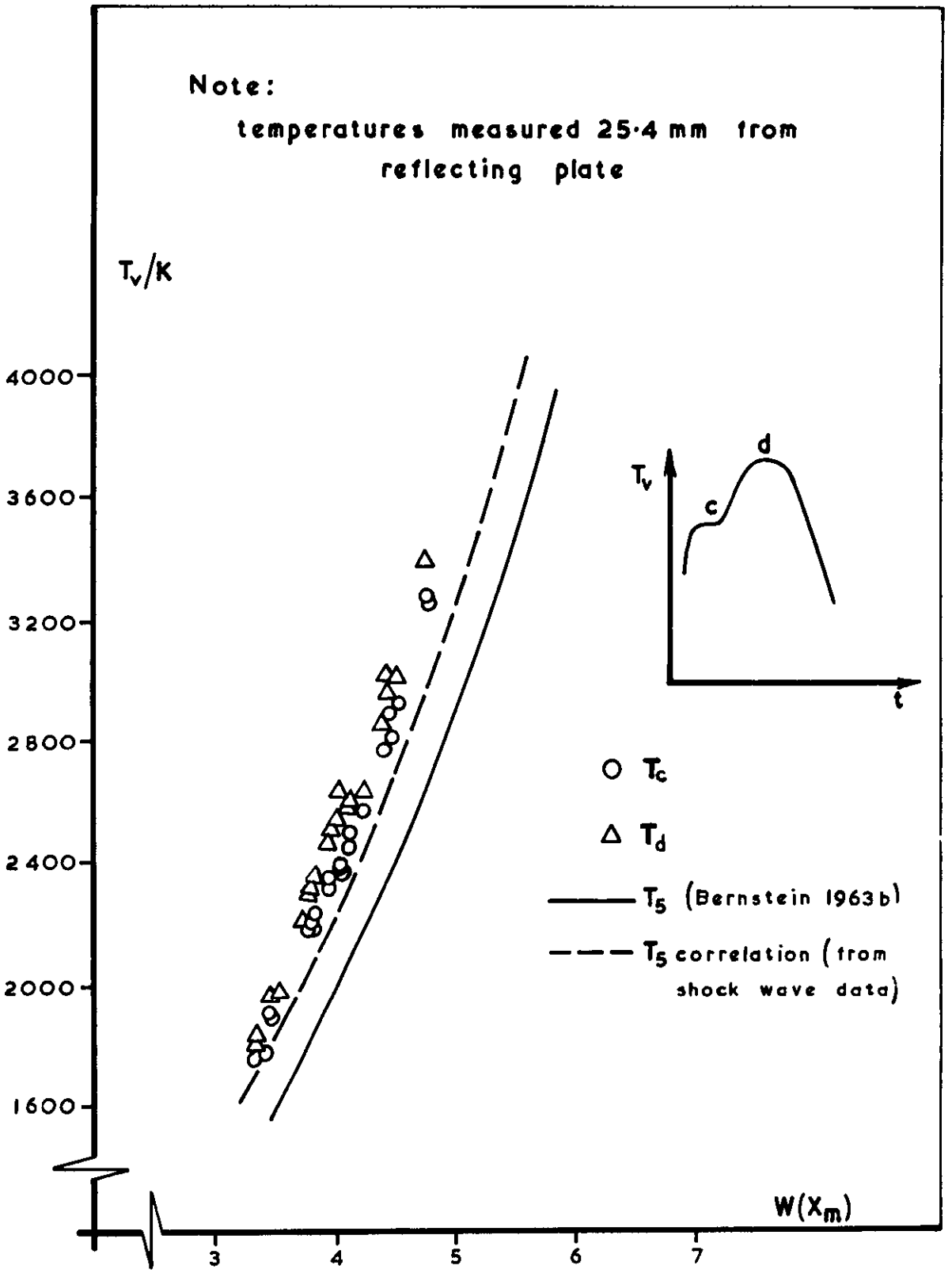

Figure 19 **Temperature variation 25·4 mm from reflecting plate**

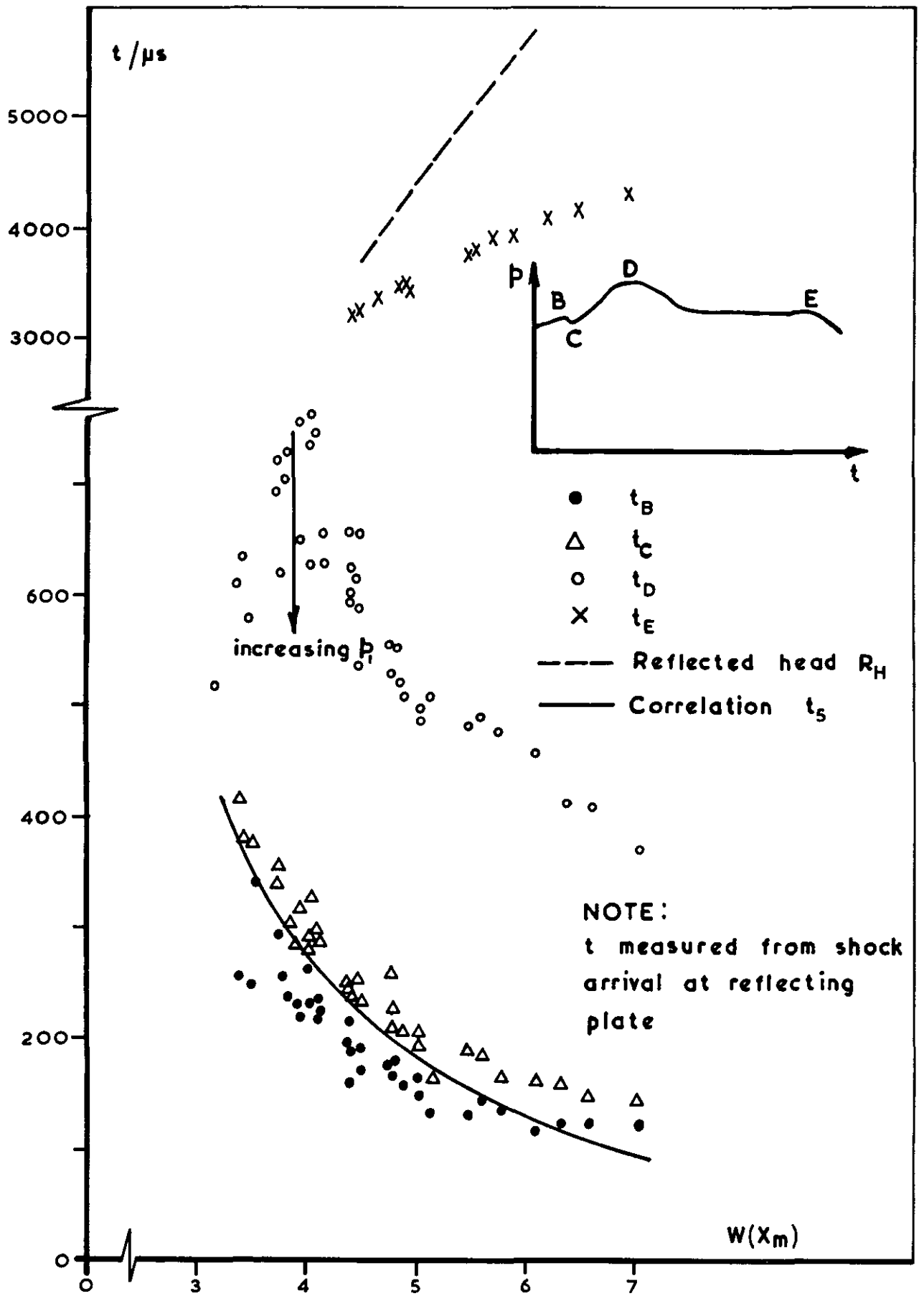

Figure 20 **Pressure duration at reflecting plate**

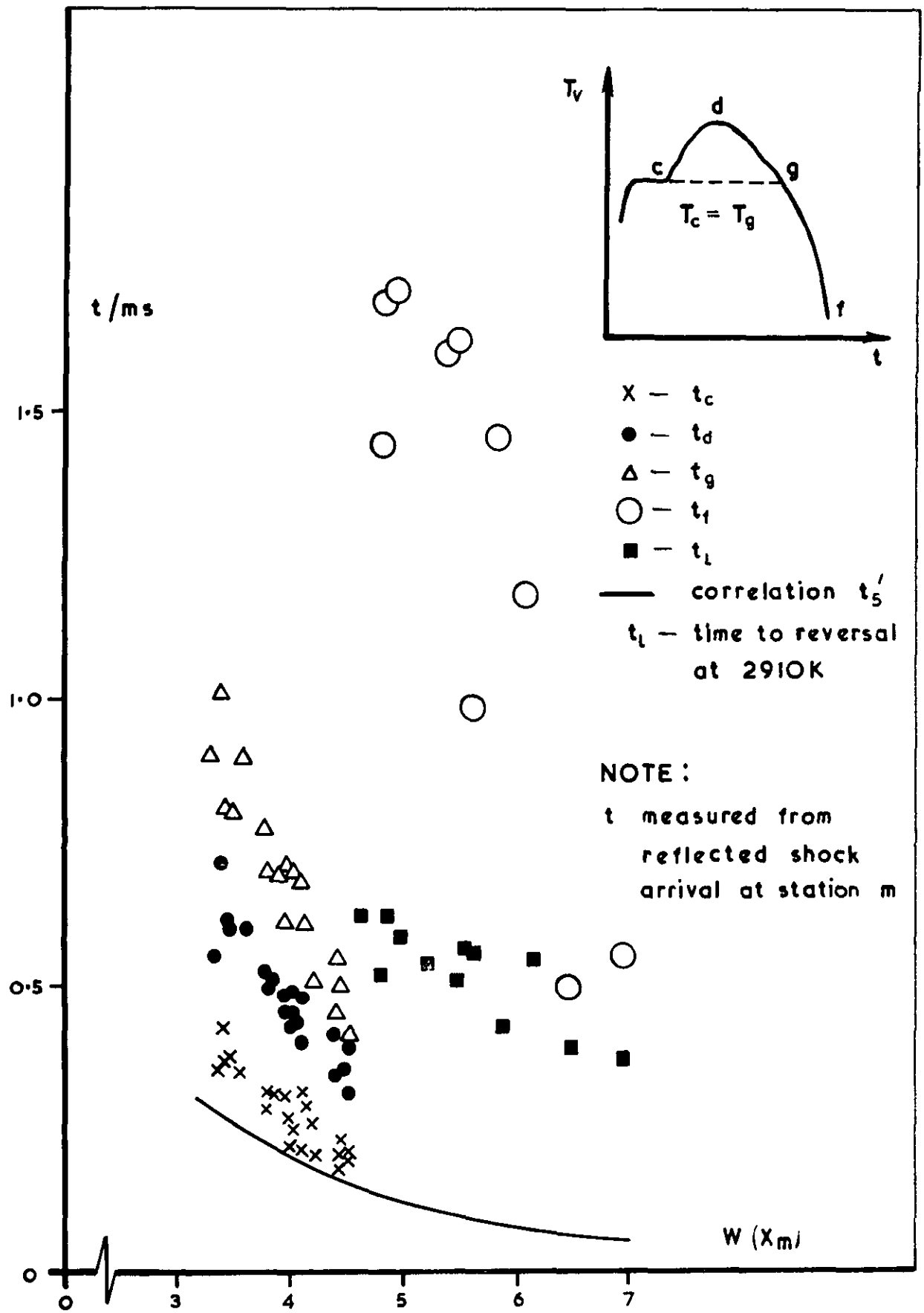

Figure 21 High temperature duration — 25·4 mm from reflecting plate

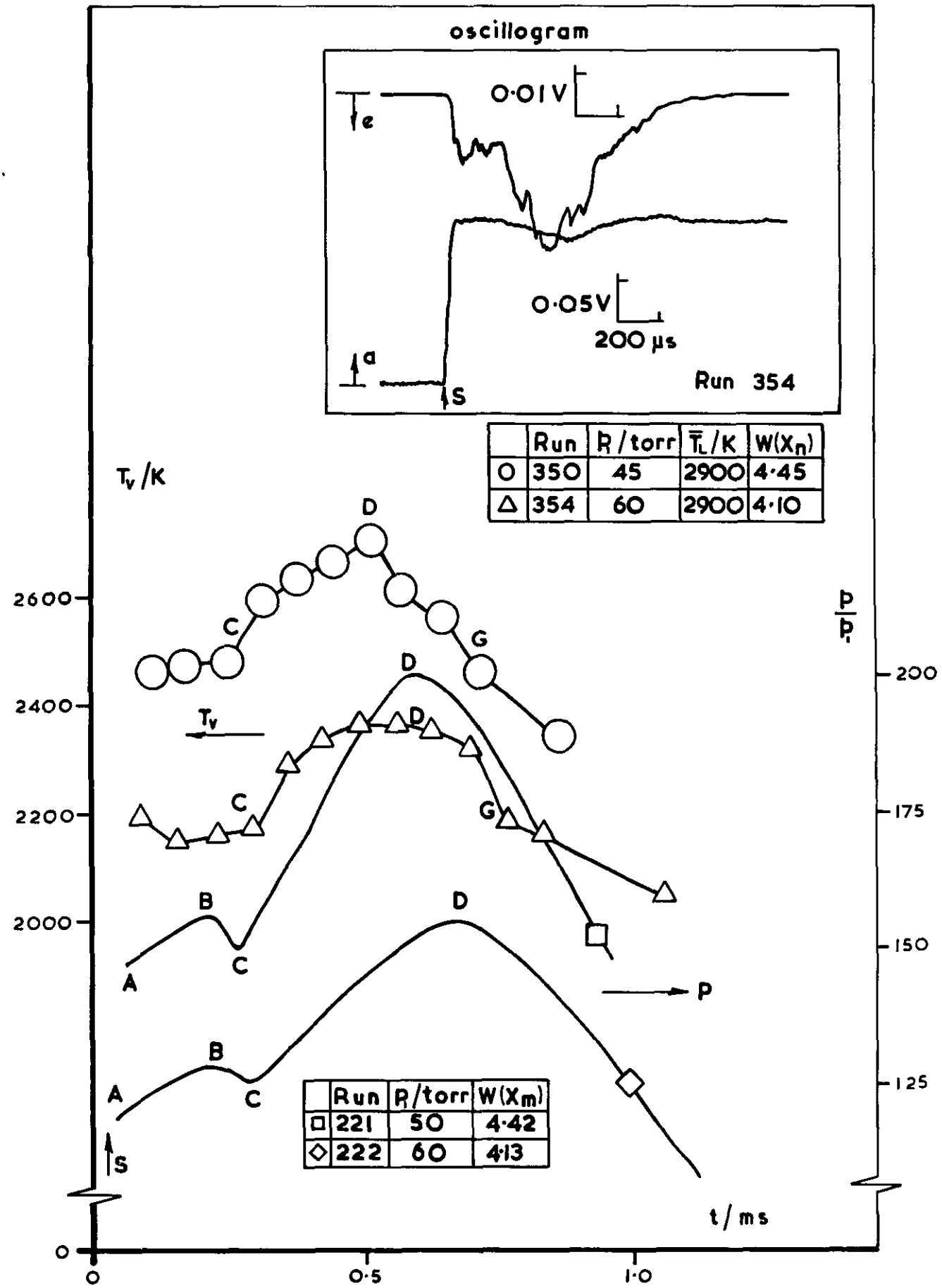

Figure 22 Temperature variation at nozzle entrance

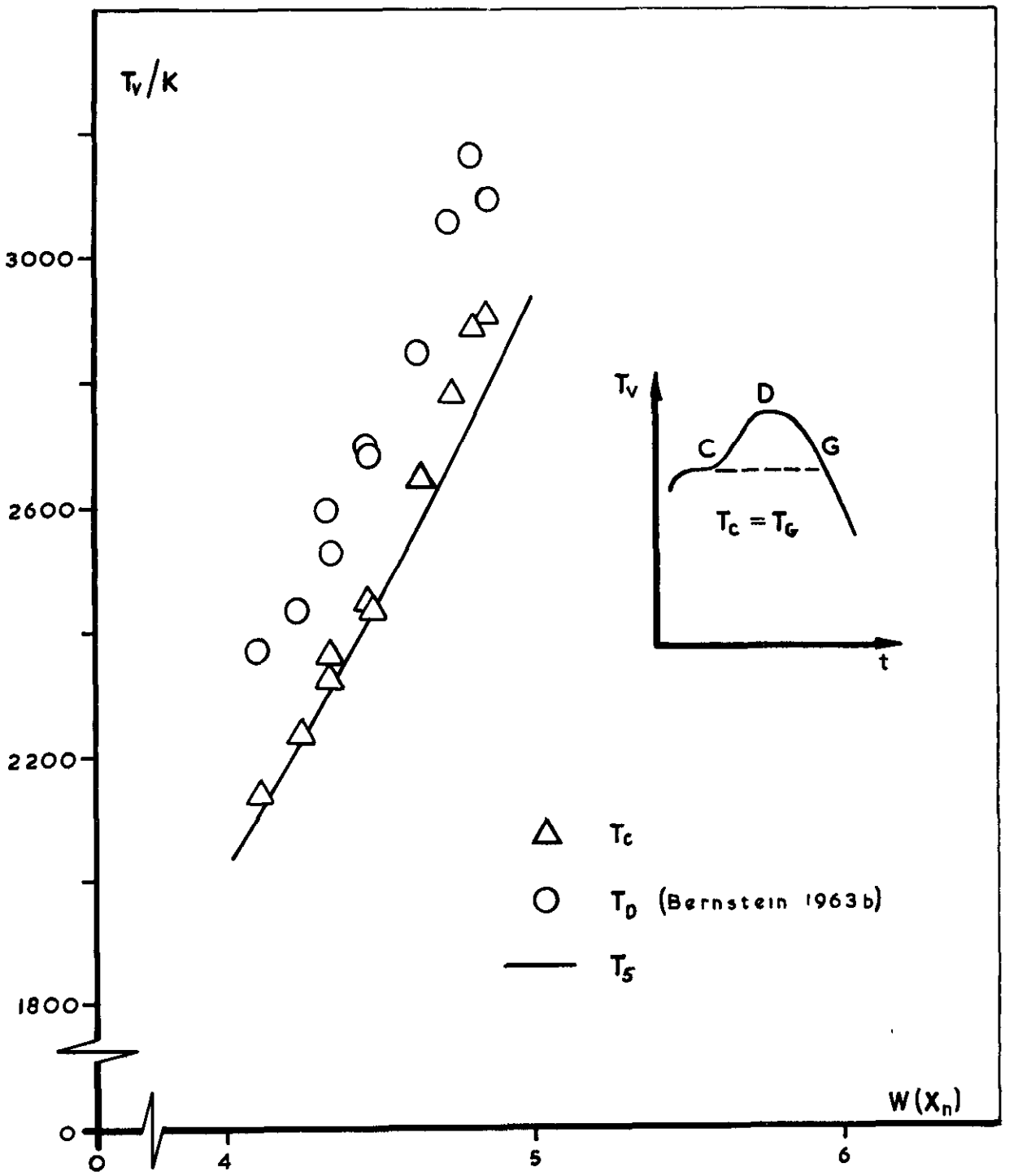

Figure 23 **Nozzle entrance temperatures**

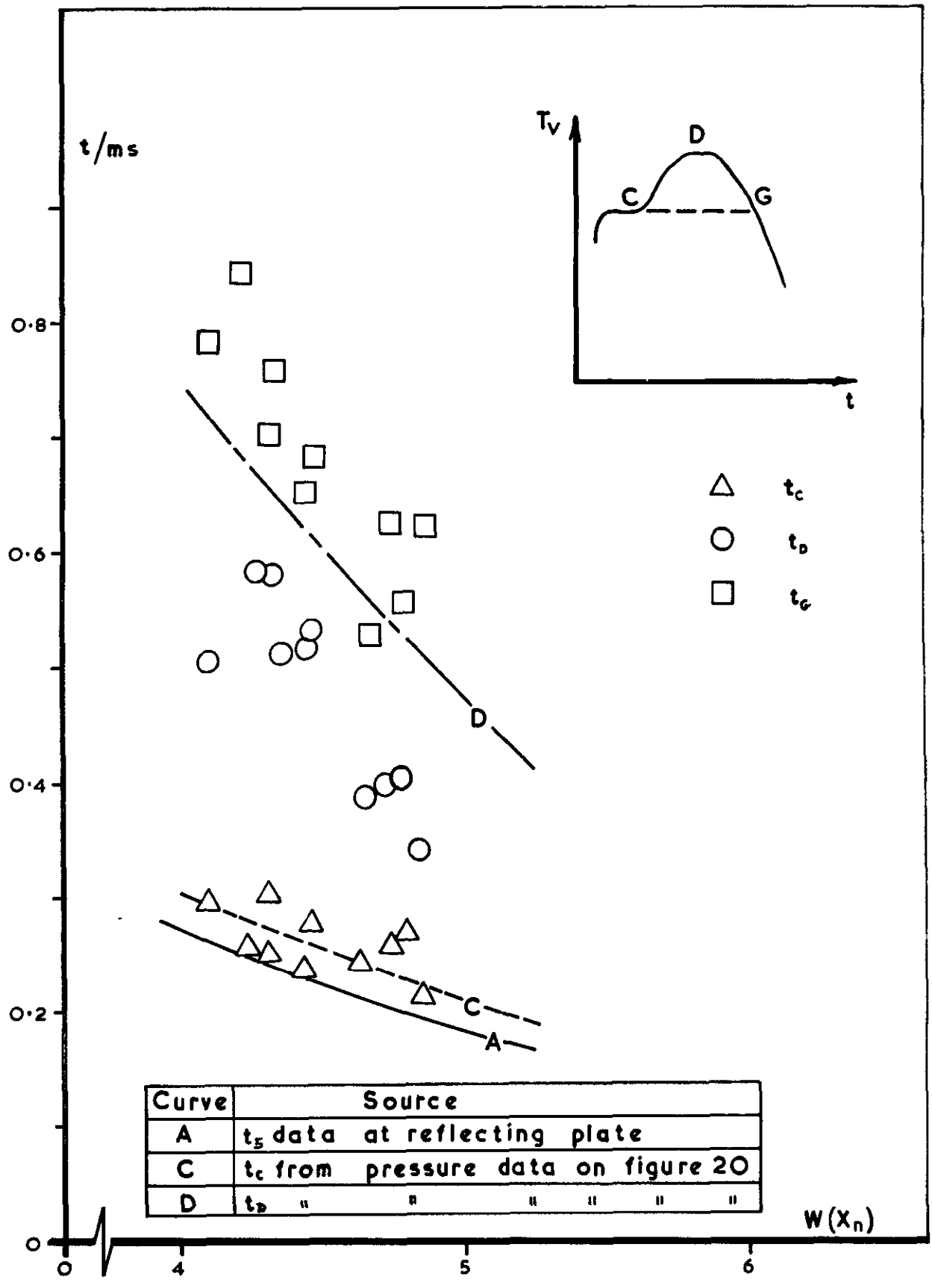

Figure 24 High temperature duration at nozzle entrance

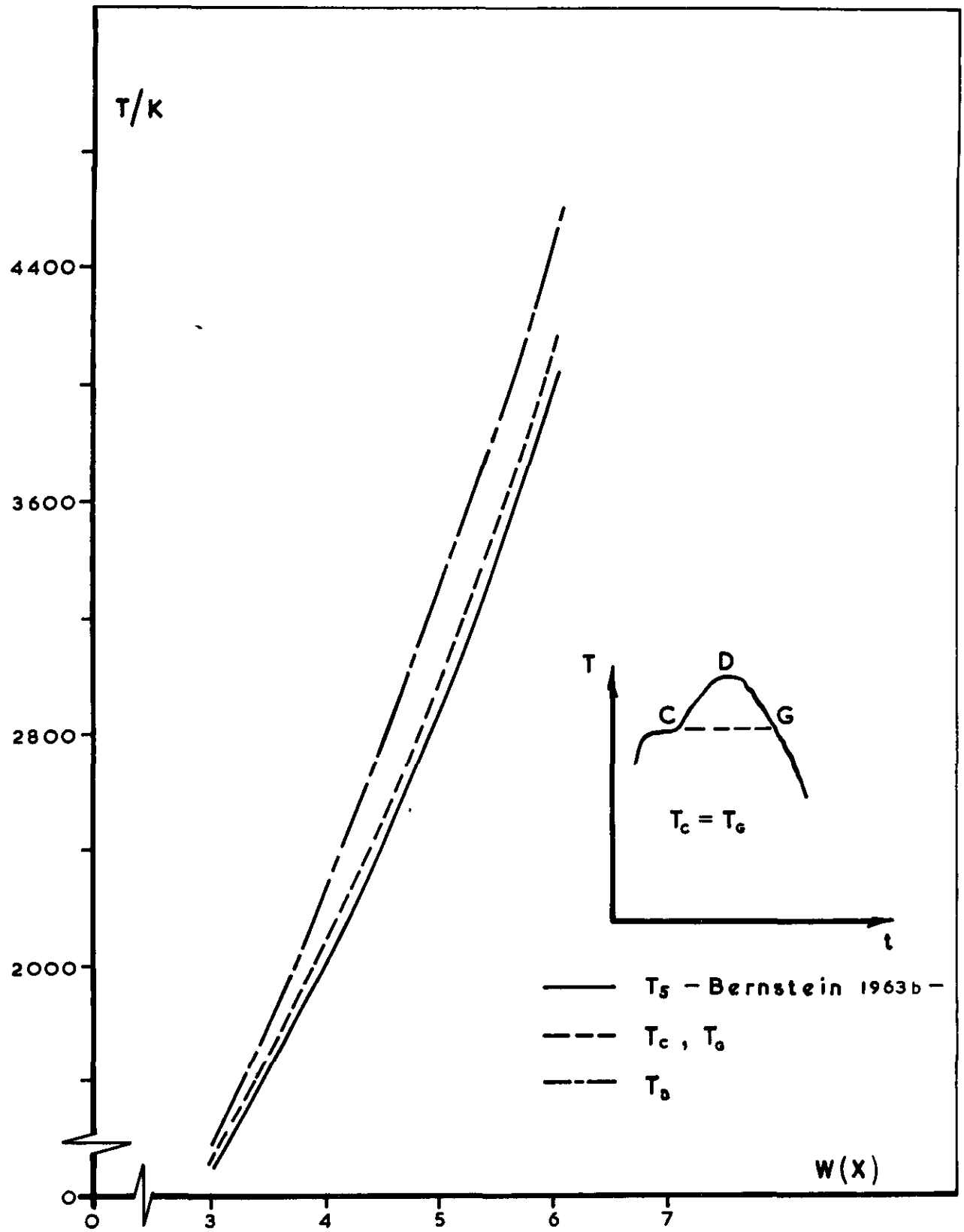

Figure 25 **Estimated temperature variation at nozzle entrance**

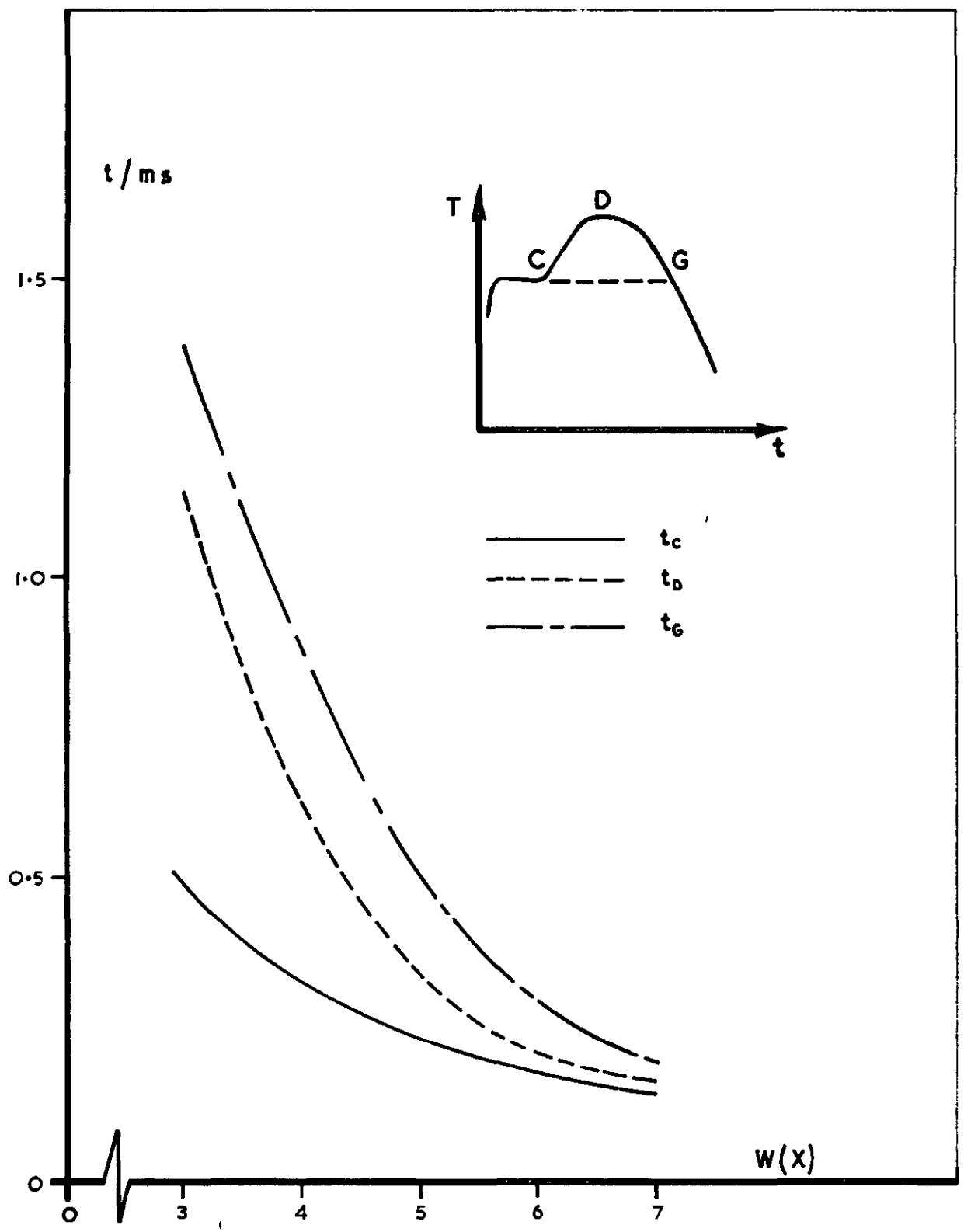

Figure 26 Estimated high temperature duration at nozzle entrance

HER MAJESTY'S STATIONERY OFFICE

Government Bookshops

49 High Holborn, London WC1V 6HB
13a Castle Street, Edinburgn EH2 3AR
109 St Mary Street, Cardiff CF1 1JW
Brazennose Street, Manchester M60 8AS
50 Fairfax Street, Bristol BS1 3DE
258 Broad Street, Birmingham B1 2HE
80 Chichester Street, Belfast BT1 4JY

Government publications are also available through booksellers

C.P. No. 1239

SBN 11 470792 8